A linear ontogeny accounts for the development of naive, memory and tumor-infiltrating regulatory T cells in mice

Sanmoy Pathak*[1], Thea Hogan*[1], Sanket Rane*[2,3], Yundi Huang[1], Claire Pearson[5], Charles Sinclair[4], Simon Barry[4], Larissa Carnevalli[4], Andrew J. Yates✣[2] and Benedict Seddon✣[1]

Affiliations:

[1]Institute of Immunity and Transplantation, Division of Infection and Immunity, University College London, Royal Free Hospital, London, UK

[2]Department of Pathology and Cell Biology, Columbia University Irving Medical Center, New York, United States

[3]Irving Institute for Cancer Dynamics, Columbia University, New York, United States

[4]AstraZeneca, Cambridge Biomedical Campus, Cambridge, U.K.

[5] Kennedy Institute of Rheumatology, University of Oxford, Oxford, United Kingdom

* These authors contributed equally

✣Address correspondence to:

Andrew Yates, Department of Pathology and Cell Biology, Columbia University Irving Medical Center, New York, United States

Benedict Seddon, UCL Institute of Immunity and Transplantation, The Pears Building, Royal Free Hospital, Rowland Hill Street, London NW3 2PP, U.K.

One sentence summary:

Self-recognition drives homeostasis and differentiation of peripheral Treg that first infiltrate the tumor microenvironment

Abstract

Regulatory T cells (Treg) are critical regulators of adaptive immunity and of the pathophysiology of anti-tumoral immunity. Treg are both generated during thymic development and induced from peripheral conventional T cells. How these distinct pathways contribute to the homeostasis of circulating Treg in health and disease remains unclear. We address this question using multiple fate mapping mouse systems and modeling. Naive and effector/memory (EM) Treg exhibit distinct dynamics but are both continuously replenished by de novo generation throughout life. The predominant precursors of circulating EM Treg are naive thymic Treg and not conventional T cells, a process driven by self rather than foreign antigen recognition. Using the same fate reporters and three tumor models we demonstrate that infiltrating Treg specifically derive from pre-existing EM Treg. In summary, we define a linear ontogeny of Treg from thymus to EM, driven by self-antigen recognition, that then gives rise to tumor infiltrating Treg.

Introduction

Regulatory T cells play a vital role in maintaining the immune system in a state of active tolerance of self-antigens (*1*) but also regulate normal adaptive immunity to pathogens (*2*), tissue homeostasis (*3*) and development of malignant disease (*4*). As such, adoptive Treg therapy is being considered for treatment of autoimmune and inflammatory conditions (*5, 6*). In malignant disease, Treg are common constituents of tumor infiltrates, and in many instances are a biomarker of poor prognosis where their suppressive activity is thought to counteract beneficial tumor immunity (*7-9*). Therapies that target regulatory T cells have been met with striking successes in the clinic, restoring anti-tumoral immunity (*10-12*). However, such treatments are also often associated with toxicity due to loss of self tolerance and specifically targeting intra-tumoral Treg remains a major challenge. Knowledge of how Treg are generated and maintained throughout life is therefore critical for fully understanding their physiological functions both in the normal healthy immune system, and for designing and predicting the long-term impact of immunotherapies targeting regulatory T cell activity.

Treg are characterized by expression of Forkhead Box protein 3 (Foxp3) (*13*) and circulate through secondary lymphoid organs and reside in tissues (*14, 15*). They are a heterogenous population in terms of ontogeny and differentiation state (*16*), and are derived from two principle sources. First, Treg develop in the thymus (*17, 18*) from precursors amongst CD4 single positive (SP) thymocytes and are termed thymic or natural Treg (tTreg). Their development is mediated by agonist recognition of self-determinants, that drives induction of Foxp3 in a CD4 SP T cells, with stable commitment supported by the cytokines IL-2 and IL-15 (*19-24*). Second, Treg also derive following induction of Foxp3 in conventional peripheral $CD4^+$ T cells and are termed inducible Treg (iTreg) (*25*). iTreg generation is characterized in vitro through activation in the presence of TGFβ(*26*), and is observed in vivo in response to foreign antigenic challenge at intestinal sites,(*27, 28*). A significant fraction of Treg that reside in the intestine derive by this route and express ROR-γt expression (*29-32*). ROR-γt^+ Treg are rare in lymphoid tissues and restricted to mesenteric lymph nodes (*30*). In malignant disease, Treg are commonly found amongst the T cell infiltrate of the tumor microenvironment (TME) (*33*). There is evidence that both iTreg and tTreg reactive to tumoral and neoantigen contribute to the intratumoral Treg pool (*29, 34*). Studies that have attempted to distinguish tTreg and iTreg phenotypically correlate low levels of Nrp1 expression with iTreg (*29, 35*) and high levels of the transcription factor Helios with tTreg(*36*), though the reliability of these markers has since been called into question (*37, 38*). The precise extent to which tTreg and iTreg contribute to the maintenance of circulating Treg pools in lymphoid tissues and recruited to tissue sites during disease remains unclear.

Peripheral Treg exhibit considerable functional and phenotypic heterogeneity. They comprise naive-like $CD44^{lo}CD62L^{hi}$ $CCR7^{hi}$ cells and more differentiated populations that display an activated $CD44^{hi}CD62L^{lo}$ effector/memory (EM) surface phenotype, markers such as Ox40, GITR, CD69, and

altered chemokine receptor expression (*39-43*). These states have also been described during elicitation of iTreg following mucosal antigen challenge and are associated with their generation and migration to mucosal sites (*31, 32, 44*). Treg can also express signature transcription factors associated with type 1 (Tbet)(*45*), type 2 (Gata3)(*46*), type 17 (ROR-γt)(*28, 29*) or T follicular helper responses (Bcl6)(*47*) and are implicated in regulating the associated T helper responses. The expression of these transcription factors appears transient rather than defining stable sub-lineages (*46*). Single cell RNAseq analysis of intratumoral T cell populations reveals even greater degrees of phenotypic heterogeneity (*48*), though determining which genetic properties represent transient responsive states, specific differentiation states, and those defining more persistent sublineages remains a major challenge.

The homeostatic mechanisms responsible for maintaining conventional T cell populations have been studied extensively, and the distinct contributions of self-renewal and de novo generation are well recognized (*49*). In contrast, the dynamics underlying the maintenance of the mature Treg pools, and in particular the contribution of thymic Treg generation, are less clear and in part obscured by their complex ontogeny. tTreg are present in the thymus throughout life, implying a role for replenishment of peripheral compartments with new cells. However, studies of Rag2-EGFP mice reveal that a fraction of these cells are mature Treg that have recirculated back to the thymus (*50, 51*), and it has been suggested these recirculated Treg compete for IL-2 and directly inhibit intrathymic Treg development (*50*)(*16*). Circulating Treg are also more proliferative than naive conventional T cells (*52*), as indicated by basal expression of the proliferation marker Ki67 (*16*), suggesting that self-renewal contributes substantially to Treg maintenance, as it does for conventional $CD4^+$ memory T cells (*53*). Further, while it is evident that Treg resident at mucosal surfaces derive from both tTreg and iTreg, the extent and dynamics of replenishment of circulating EM Treg, and the identity of their precursor(s) are far less clear. In total, considerable uncertainty remains regarding how circulating Treg are generated and maintained, and how these processes might impact their function during immune challenge.

Here we sought to better understand the homeostatic mechanisms that are responsible for maintaining the circulating pool of Treg. There are currently no reliable markers or a single fate-mapping approach that can distinguish and track tTreg and iTreg. In this study we employed multiple and independent fate mapping systems to define the ontogeny, temporal dynamics and maintenance of circulating Treg pools across the mouse lifespan and used these same systems to understand the generation and recruitment of Treg in the setting of malignant disease.

Results

Thymic Treg comprise both *de novo* generated and recirculated mature cells

To understand the dynamics of circulating regulatory T cells we performed temporal fate mapping using busulfan drug-conditioned bone marrow chimeric mice (*54*). In this model, busulfan specifically ablates the B6.CD45.1 host hematopoetic stem cell (HSC) compartment, allowing its reconstitution with congenically labelled B6.CD45.2 donor stem cell progenitors. Importantly, mature hematopoetic lineages are unaffected by this conditioning, allowing one to measure the healthy, constitutive influx of new cells into existing replete compartments to be detected and measured over time. The kinetics and extent of replacement in any given cellular compartment are rich in information about the dynamics of its maintenance (*54-57*). To assess potential host age effects upon Treg homeostasis, chimeras were generated with hosts of a range of ages (6-8wks, 8-10wks, 10-12wks and 12-25wks). We then analyzed Treg phenotype in thymus, lymph nodes and spleen of chimeras between 14 and 300 days post-BMT. The extent of HSC reconstitution (donor chimerism) was assessed by measuring the donor fraction amongst CD4 CD8 double positive (DP) thymocytes, which stabilizes within 5 weeks after BMT and serves as an accurate proxy of average HSC chimerism across all bone marrow sites (*58*). Following busulfan treatment, donor fractions amongst DP thymocytes were between 70-100% (Fig. 1A). Normalizing the observed donor fraction in any downstream population to the equilibrated donor fraction in DP thymocytes accurately reflects the extent to which that population has been replaced through de novo hematopoesis since BMT.

We first analyzed the dynamics of Treg development in the thymii of both untreated WT and busulfan chimeras (Fig. 1B). In mice, thymic size and output peaks at around 6 weeks of age, after which the thymus undergoes a slow but steady atrophy (*59*). Measuring total numbers of DP and CD4 single positive (CD4SP) thymocytes in control mice and chimeras confirmed the expected peak and subsequent decline in numbers (Fig. 1C). We have previously estimated that these populations wane exponentially with age, halving in size approximately every 150d (*54*). In contrast, total Foxp3$^+$ Treg numbers in the thymus showed no significant decline with age (p=0.15, Fig. 1C). We confirmed the presence of thymic Treg of both naïve and EM phenotypes (Fig. 1B). However, this composition shifted over time; naive Treg numbers declined significantly with age (Fig. 1D), while EM Treg numbers increased, reaching a plateau around 9 weeks of age and remaining relatively stable thereafter (Fig. 1D). To confirm the ontogeny of these intrathymic populations, we next analyzed the influx of donor-origin cells into these subsets over time, in busulfan chimeric mice. The normalized donor fraction within CD4SP thymocytes rapidly reached 1 within a few weeks post BMT, indicating that this population had turned over completely (Fig. 1E). Naive thymic Treg also underwent rapid replacement by donor progeny, but only to a level of ~80% (Fig. 1E). In contrast, donor-origin EM Treg were not readily detectable until almost 100 days post BMT, even though numbers of memory

Treg in the thymus peaked by ~d63 of age. The presence of host-derived naive and memory Treg within the thymus validates the conclusion that these Treg are not de novo generated but recirculated from the periphery. Previous studies have suggested that mature Treg that recirculate in the thymus compete for IL-2 and thereby impair de novo Treg generation (*50*). To quantify any such inhibition in our experiments, we needed knowledge of the donor:host compositions of both recirculating and newly-generated naive Treg. We therefore assessed the dynamics of Treg turnover in the periphery.

De novo production of naive thymic Treg continues with age

We analyzed peripheral naive and EM Treg subsets in lymph nodes and spleen of both WT mice and busulfan chimeras, measuring donor/host chimerism and Ki67 expression (Fig. 2A). From birth, total numbers of naive Treg rose rapidly in young mice, reaching maximal levels as early as 5 weeks of age. Numbers were maintained for several months after which a gradual decline was evident (Fig. 2B). In contrast, EM Treg were scarce in young mice, but gradually increased in number until 9-10 weeks of age, and accumulated more slowly thereafter (Fig. 2C). Correspondingly, naive:EM Treg ratios in both LN and spleen were high early in life but declined progressively, with memory Treg exceeding naive Treg numbers at around 8 months of age (Fig. 2D). Analyzing the kinetics of donor cell influx in busulfan chimeras also exposed distinct dynamics. Naive Treg were initially replaced rapidly and reached a plateau of approximately 70% replacement by d100 (Fig. 2E). In contrast, donor influx into the EM Treg pool was much slower and reached a far lower level of replacement (Fig. 2E). Ratios of donor chimerism between LN and spleen of individual mice remained close to 1 in both naive and EM Treg, throughout the time course (Fig. 2F) suggesting that naive and EM Treg are largely independent and freely recirculating populations in lymphoid tissues.

The failure of donor naive Treg to completely replace host counterparts in the thymus strongly suggested that some fraction of naive thymic Treg had recirculated from the periphery, in addition to the recirculation of EM Treg. To estimate this fraction, we assumed that the donor/host composition of recirculated naive Treg in the thymus matched that of peripheral naive Treg in each individual. The additional fraction of donor naive Treg observed in the thymus would therefore represent de novo generated thymic Treg. We estimated this additional fraction (Fig. 2G) and showed that at early time points after BMT, most naive Treg are de novo generated, but over time their representation declines. Earlier studies demonstrated that the fraction of total Foxp3$^+$ thymic Treg expressing Rag2-GFP collapsed dramatically with age. Estimating this fraction from our data, assuming all EM Treg were recirculated, yielded comparable results (Fig. 2H). However, the increasing numbers of Treg that recirculate to the thymus with age, together with the natural atrophy of the thymus, obscures the extent to which de novo Treg generation changes with age. To explicitly measure this change, we calculated the ratio of estimated de novo naive Treg to the size of the total CD4 SP precursor pool. In young mice, de novo generated naive Treg make up ~1% of of total CD4 SP, with a modest but significant reduction with age (Fig. 2I). Nevertheless, this analysis reveals that production of naive

Treg in the thymus continues even in aged mice and in the presence of ever-increasing numbers of mature recirculated Treg.

Thymic export and self renewal both contribute substantially to the homeostasis of naive Treg

This empirical analysis revealed that the naive and EM Treg compartments exhibited distinct shifts in their size and rates of influx of new cells with age. To better understand these dynamics, we used mathematical modeling to quantify the processes of influx, self-renewal, and loss that underlie them. We first analyzed the naive Treg compartment, comparing the support for two simple models (Fig. 3A); a 'homogeneous' model in which all naive Treg exhibit identical dynamics, and an 'incumbent' model, in which host naive Treg are heterogeneous, comprising a subset that shares the same homeostatic dynamics as newly generated donor thymic Treg, and a subset that is resistant to displacement by new donor Treg and may exhibit distinct rates of division and loss (SI Section S1A). Previously we found support for this 'first-in, last-out' structure within conventional naive T cells (*54, 57, 60*). An important observation that the models needed to explain was the failure of donor cells to achieve complete replacement of host cells. The homogeneous model predicts complete turnover of a population given consistent influx of new cells and sufficient time, which we have observed in other lymphocyte populations (*58*). Therefore, this model can only explain incomplete turnover if the steady decline in de novo generation of naive Treg, which we and others (*50*) have demonstrated, is sufficiently fast. Incomplete replacement is also explained naturally by the presence of incumbent, host-derived naive Treg, established before BMT, which persist independently of newly generated cells.

We fitted each model simultaneously to the time courses of total numbers of naive Treg, their host/donor composition, and the levels of Ki67 expression among donor and host cells (Fig. 3B). We assumed that the fluxes of host and donor cells into the naive Treg compartment were proportional to the numbers of their respective de novo generated thymic naive precursors, the time courses of which we described empirically (SI Section S1C and Fig. S1). While both models captured the changes in the total numbers of naive Treg with age (Figs. 3B and 3C, left panels), the homogeneous model could not account for the incomplete donor influx (Fig. 3B, right panel), even given the waning production of new naive Treg by the thymus (Fig. 2I, S1). This model also failed to account for the higher frequency of Ki67 expression among host cells than among donor cells (Fig. 3D). In contrast, the incumbent model provided better descriptions of these key observations (Fig. 3E), indicating that the naive Treg compartment is heterogenous with respect to its propensity for replacement. Formal evaluation of model fits substantiated this view, with statistical analysis revealing significant support (model weight = 99%) for the incumbent model compared to the homogeneous model (see SI section S3 for details). This simple model of heterogeneity predicted that displaceable naive Treg had a

mean residence time of around 40 days and divided on average every 60 days (Fig. 3F), whereas incumbent Treg, which were assumed to be stable in numbers, divided and were lost every 20 days. The displaceable naive Treg population was sustained by influx from thymic precursors throughout life (Fig. 2E). However, the contribution of self-renewal becomes increasingly important as mice aged, a contribution estimated to increase to close to 70% in mice over a year old as precursor numbers declined (Fig. 3G). In tandem, incumbent cells made up an increasing proportion of the population with age (Fig. 3H). This kinetic explains the diverging levels of Ki67 expression among donor and host cells with age (Fig. 3D).

Modeling of EM Treg dynamics favors naive Treg as the direct precursors

Next, we extended our modeling approach to investigate the ontogeny and homeostasis of EM Treg. While our data and others clearly suggest that naive peripheral Treg derive directly from thymic naive Treg, the extents to which EM Treg derive from naive Treg or are induced from conventional T cell subsets is unclear. We therefore explored models in which the precursors of EM Treg are either naive peripheral Treg, or are instead iTreg, deriving from a Foxp3-negative conventional T cell subset; either naive ($CD44^{lo}CD62L^{hi}$), central memory ($CD44^{hi}CD62L^{hi}$), or effector memory ($CD44^{hi}CD62L^{lo}$) cells. Irrespective of the precursor, we reasoned that differentiation into EM Treg occurs through T cell activation and subsequent division. Therefore we explored a simple two-compartment model in which precursors enter the EM Treg compartment via a fast dividing subset, behavior that resembles acutely activated T cells that divide and turn over quickly, before differentiating to a more quiescent, slowly dividing population, that represents a resting state post-activation with lower rates of division and death reflecting normal homeostatic processes (Fig. 4A). Previously we found support for similar behavior within circulating conventional memory CD4 T cells (*55, 56*). SI Section S1B provides a detailed description of the two-compartment model. To define the influx into host and donor EM Treg in this model, we used empirical descriptions of the time courses of the numbers and donor chimerism of candidate precursors of memory Treg (Fig. S2). By fitting this model to the total numbers of EM Treg as well their donor/host composition and Ki67 levels, we found modest support (52%) for naive Treg as their primary precursor, over TEM (26%), TCM (13.5%), and naive Tconv (8.5%; see SI Section S2 for details). Nevertheless, this best fitting model was able to explain the changes of EM Treg numbers with age (Fig. 4B) and the kinetics of their replacement by donor cells (Fig. 4C). The model also explained the greater expression of Ki67 amongst donor cells than host cells at early times after BMT (Fig. 4D), when donor cells are more prevalent within the more recently recruited fast-dividing subset. Self-renewal did not compensate for the loss of fast-dividing cells (Fig. 4E), indicating a role for influx in driving the accumulation of EM Treg during the first year of life; this influx represented approximately 1% of EM Treg per day, although this proportion declines with age (Fig. 4F). We estimated that cells persist in the fast-dividing state for about a week before transitioning to a slower-dividing state, consistent with the

normal dynamics of T cell activation, and that slowly dividing EM Treg divide and die on average roughly every 40 days (Fig. 4E). From this similarity in rates of self-renewal and loss we predict that cohorts of slow EM Treg can persist dynamically (that is, at a clonal or population level) for many months. The model also explains the increase in total numbers of EM Treg during the first year of life (Fig. 4B); during this period, even though the total rate of influx of new memory from its precursor is declining, it still outstrips the net rate of loss of fast-dividing cells, continually boosting their numbers. This accumulation in turn drives the accumulation of slow EM cells, explaining the decline in Ki67 among EM Treg in bulk across the same period (Fig. 4D). See SI section S1D for details.

Foxp3-CreER temporal fate mapping supports naive Treg as the primary source of EM Treg

To test the conclusion that naive Treg are the precursors of recirculating EM Treg, we used a *Foxp3*$^{GFP\text{-}CreERT}$ *Rosa26*^{RmTom} fate reporter strain (Foxp3FR hereon). Induction of CreERT activity by a single dose of tamoxifen (TAM) induces permanent and heritable mTom expression in approximately 75-80% of Foxp3$^+$ cells (Fig. 5A). Following TAM administration, the fraction of Foxp3$^+$ CD4$^+$ T cells labelled with mTom declined gradually (Fig 5A). Foxp3-GFP and CD25 expression by mTom-labelled cells confirmed that reporter induction was restricted to Foxp3$^+$ cells. Consistent with earlier studies (*61*), mTom+ cells retained a CD25^{hi}Foxp3$^+$ phenotype throughout the chase period (Fig. 5A), confirming Treg lineage fate was stable in the steady state over time. The decline in mTom+ cells among naive Treg after treatment was expected, as our analysis of busulfan chimeras showed that naive Treg are continuously replaced by newly generated cells from the thymus (Fig. 2C). We fitted a smooth curve (spline) to the kinetic of host cell replacement in busulfan chimeras (Fig. 2E) and overlaid this curve on the time course of the observed mTom-negative fraction, aligned to the 20% level that is the baseline mTom labelling (Fig. 5B, dashed line). The subsequent kinetics were in good agreement, validating the conclusions we drew from the busulfan chimeric mice. To test our assertion that naive Treg, rather than naive conventional T cells, are the primary precursors of EM Treg, we followed mTom expression among EM Treg following TAM treatment of Foxp3FR mice. Because only Foxp3$^+$ Treg were labelled with mTom (Fig. 5A), we reasoned that the kinetics of dilution of mTom-expressing EM Treg would be slow if newly generated EM Treg derived from a labelled precursor (i.e. pre-existing Treg) or fast if precursors were instead unlabeled (i.e. conventional T cell). In busulfan chimeras we saw that almost ~40% of EM Treg were replaced by new influx between d25 and d150 post BMT. In TAM-treated Foxp3FR mice, we did not observe any significant infusion of the mTom– cells into EM Treg over a similar timeframe (Fig. 5C), indicating that cells entering the EM Treg pool in this interval must be rich in mTom+ cells. The most parsimonious explanation for these dynamics is that naive Treg are indeed the predominant or exclusive source of EM Treg in the steady state.

Constitutive EM Treg development is driven by self recognition, independently of microbiome

Our data from busulfan chimeras demonstrated that EM Treg are continuously generated throughout life, via a Ki67^{hi} intermediate, strongly suggestive of an activation linked cell division process. This led us to consider the identity of the antigens driving this continuous EM Treg generation. Given that naïve Treg are selected on self-antigens in the thymus and have an intrinsic ability to recognize spMHC, it is possible that recognition of self-antigens in the periphery is also implicated in driving EM Treg generation. Alternatively, interactions with foreign antigens from the microbiome could drive EM Treg generation, as has been described in the gut mucosa (*31, 32, 44*). We explored these possibilities in two ways. First, we studied germ free (GF) mice, which are completely devoid of microbiota. One developmental consequence of their gnotobiotic state is that GF mice lack normal lymph node structures. Therefore, we compared the numbers and phenotype of Treg found in the spleens of GF mice with those from conventionally housed WT mice. GF mice contained normal numbers of both naive and EM Treg (Fig. 6A). Turnover of these populations, assessed by Ki67 expression, also appeared normal in the absence of microbiota (Fig. 6A).

Second, we took advantage of a natural experiment that occurred when our mouse colony was relocated from a facility using open cages and conventional diets and tap water (which we refer to for brevity as “dirty”) to a new (“clean”) facility in which mice were housed in individually ventilated cages and fed sterile irradiated diet and water. The data presented in Figs.1-2 were generated from mice held in the clean facility. However, similar experiments were conducted in the dirty facility prior to relocation, and showed that memory compartments of conventional T cells are substantially enlarged in mice held in dirty conditions, and that the natural microbiota play a critical role in establishing compartments of conventional memory cells in mice (*56*). The enlargement of memory compartments observed in these mice is comparable to that described in other models of “dirty” mice, such as wildling mice (*62*) and mice co-housed with pet-shop mice (*63*). As further illustration, the ratio of memory:naive conventional T cell populations in dirty hosts was elevated throughout life, compared with clean hosts (Fig. 6B). We therefore performed a meta-analysis to examine the steady state generation of naive and EM Treg in busulfan chimeras housed in dirty and clean settings. Comparing the normalized donor fractions in the two sets of chimeras revealed similar trajectories of donor cell influx into both naive and EM Treg subsets (Fig. 6C). Similarly, the kinetics of total donor Treg numbers that are generated following BMT confirmed this view, with absolute numbers of naive or EM donor Treg reaching identical levels in both clean and dirty hosts (Fig. 6D). Together these results demonstrate that the tonic generation of EM Treg occurred independently of host microbiota.

Tumor infiltrating Treg derive from existing circulating EM Treg

Our results suggest that self-recognition drives a linear pathway of development of naive and EM Treg throughout life. We next asked how these dynamics applied in the context of malignant disease setting. Previous studies of MC38 tumors in mice characterize infiltrating Treg as being induced from conventional T cells and are identified by their low expression of the marker Nrp1 (CD304)(*29*). We therefore examined the lymphocytic infiltrate of MC38 tumors engrafted into our different fate reporter models to more directly characterize the ontogeny of tumor infiltrating Treg.

We first used the Foxp3FR reporter strain to determine whether Treg in TME derived from pre-existing Foxp3$^+$ Treg, or were induced from conventional T cells, following tumor grafting. Foxp3FR mice were treated with TAM to pre-label existing Foxp3$^+$ Treg, and then were engrafted several weeks later with MC38 cells. Analyzing cellular composition of tumor masses at maximal tumor size (~d17) revealed the anticipated lymphocytic infiltrate of T cells (Fig. 7A). CD4$^+$ T cells in the TME included a substantial fraction of Foxp3$^+$ Treg that exhibited an activated EM phenotype with evidence of elevated activation state, since PD1 and Ki67 frequencies were increased compared to naive and EM Treg from LN or spleen (Fig. 7B). Consistent with previous reports (*29*), Nrp1 expression levels were modestly reduced on tumor infiltrating Treg (Fig. S3). Examining Foxp3 reporter expression by Treg in TME revealed that in all cases a large proportion of Treg recovered from tumors expressed mTom, indicating that they derived from Treg labelled prior to tumor engraftment. Furthermore, the frequency of mTom expression by Treg in tumor was like that of Treg from lymphoid tissues of the same host (Fig. 7B). Over the course of the experiment, mTom frequencies in naive and EM Treg compartments of LN and spleen diverged, as mTom-negative cells more rapidly replenished the naive Treg pool. A closer inspection of mTom frequencies revealed expression among tumor-infiltrating Treg was similar to the maximum level observed shortly after TAM treatment, that also remained high amongst EM Treg, implying that tumor-infiltrating Treg predominantly derive from circulating EM Treg. To explore this ontogenic relationship further, we performed temporal fate mapping of Treg in the TME to assess their origin. To do this, we exploited the fact that donor derived cells accumulate in naive and EM Treg with highly distinct kinetics (Fig. 2E). A concordance of the donor fraction of Treg in TME with either naive or EM Treg would reveal the Foxp3$^+$ precursor of intratumor Treg. Chimeras were generated as described earlier and were engrafted with MC38 cells at 8 weeks post BMT. At this time, the donor fraction among naive Treg was ~0.4 but was much lower (~0.1) among EM Treg. Measuring the donor fraction among Treg from tumors revealed low chimerism, closely resembling that of circulating EM Treg (Fig. 7C). These data strongly suggest that Treg infiltrating MC38 tumors derived from pre-existing EM Treg.

Finally, we asked whether this ontogeny was applicable to other tumors. We therefore analyzed Treg infiltrates in two other model tumor systems, EL4 (thymoma) and A20 (B cell malignancy) in TAM treated Foxp3FR hosts. In both cases, Treg recovered from the TME were EM phenotype, with

elevated Ki67, and expressed the mTom reporter at a level that correlated closely with circulating EM Treg in the same host (Fig. 7D). These observations demonstrate that the tumor-infiltrating Treg derived from cells that had already committed to a regulatory phenotype.

Discussion

Using independent fate reporter systems to track development and differentiation of Treg, our results strongly support a linear model of Treg development driven by self-recognition. Thymus-derived Treg continually replenish circulating naive Treg throughout life, and these in turn differentiate into the circulating EM Treg pool constitutively throughout life, driven by self-recognition. Following tumor engraftment, we found strong evidence that the large majority of tumor-infiltrating Treg derive specifically from circulating EM Treg. As such, we found that the homeostasis of circulating Treg, both in health and malignant disease, is well accounted for by production and differentiation of thymically derived Treg and does not rely upon a substantial contribution from iTreg.

Given the deleterious impact of suppression of anti-tumoral responses (*7-9*), the origin of regulatory T cells recruited to tumors has been a subject of intense study in recent years. Studies that suggest a significant contribution of inducible Treg to intratumor infiltrates have largely relied on correlative data, using markers or transcriptional profiles thought to distinguish iTreg and tTreg (*29, 36*), or the overlap of TCR repertoires within recirculating Treg and Treg from the TME (*64*). These approaches can be problematic since markers such as Nrp1 do not always correlate well with the apparent origin of Treg (*37*). Further, the TCR repertoires of populations within the TME will inevitably be shaped by the activation events driving their recruitment and retention, making comparisons with putative precursor populations difficult, and conclusions are inevitably qualitative. By genetic labelling of Foxp3$^+$ Treg prior to engraftment we could clearly demonstrate that reporter expression by Treg in the TME matched that of circulating Treg. While we cannot completely exclude a contribution of de novo generated iTreg in these models, any contribution would at best represent a small fraction, given the high concordance of fate reporter between EM Treg and intratumoral Treg.

Our data also identify self-recognition as a defining property controlling circulating peripheral Treg homeostasis. The role of agonist selection in generating thymic Treg is well recognized, as is the importance of mucosal antigens, including microbiota, in driving development of RORγt-expressing iTreg in the gut (*29, 31, 32*). These cells are preferentially retained within the GI tract where they play a critical role in maintaining tolerance to the symbiotic microbiota of the gut and are only present as a small fraction of Treg in mesenteric lymph nodes that drain the intestines, and absent from other lymph nodes or the spleen. Our analysis of WT mice and busulfan chimeras show that EM Treg are generated continuously throughout life. Although the circulating Treg compartment is dominated by thymus-derived naive Treg early in life, EM Treg numbers increase steadily with age, coincident with a decline in thymic output. We saw almost half the EM Treg compartment is replaced by newly generated EM Treg by ~d160 post-BMT, and the kinetics of *Cre* reporter expression in Foxp3FR mice indicated these cells derive from naive Treg precursors. Strikingly, this tonic generation appears to occur independently of microbiota, since EM Treg were present in normal numbers in GF mice, and the kinetics of de novo production of EM Treg were identical in

"dirty" facilities that were sufficient to induce substantial inflation of conventional memory T cell subsets (*56*). Given that thymically derived naive Treg are selected on self-antigens, it seems reasonable to conclude that EM Treg development is also driven by a peripheral self-recognition event. However, it appears that only a subset of the naive Treg repertoire has the capacity to develop into EM Treg. This heterogeneity may reflect differences in either the diversity or abundance of self-antigens expressed in peripheral lymphoid tissues, as compared with the thymus, where self-antigen expression by medullary thymic epithelial cells is facilitated by AIRE (*65*). There have, however, been reports of AIRE-expressing ILC3 in lymph nodes (*66*), that may represent an additional source of self-antigens that promote EM Treg development from naive Treg precursors in peripheral compartments. The distinct ontogenies of Treg in the gut and the circulation likely reflect the different functions of these compartments, either maintaining tolerance to foreign microbiome antigens at mucosal surfaces or systemic tolerance to self-antigens. The specificity of circulating EM Treg, however, is especially pertinent to malignant diseases since T cells infiltrate tumors from the circulation. Our analyses showed that Treg in the TME derive specifically from pre-existing EM Treg, already primed by self-antigens in the periphery, rather than through neoantigen-driven activation and recruitment of either naive Treg or inducible Treg derived from conventional T cells.

Previous studies have suggested that Treg recirculating to the thymus exert negative feedback upon thymic Treg development (*50*). Our estimates of newly produced Treg as a fraction of total thymic Foxp3$^+$ T cells were in close agreement with these earlier results. However, there were two confounding issues that contrived to exaggerate the apparent decline in thymic Treg development. First was the accumulation of EM Treg in thymii, which reached a maximal level by 60 days of age. Second was thymic atrophy that progressively reduces the rate of de novo generation of thymic Treg, due a decline of precursors. Relating de novo Treg numbers to the size of the upstream precursor pool, CD4SPs, revealed stable levels of de novo Treg development for the first 8 months, with evidence of modest reduction by one year of age. The kinetics with which recirculated Treg accumulate in the thymus and the apparent reduction in Treg development do not correlate well. Given the age-related changes that take place during thymic atrophy (*67*), it is possible that the modest reduction in Treg output may instead reflect alterations in the function of some other component of thymic function such as mTECs, that are important for Treg development (*68*). Analysis of donor influx of peripheral naive Treg pools in busulfan chimeras did, however, exhibit a clear ceiling on the extent of replenishment possible, at around 0.75. A reduced thymic output of naive Treg with age could account for this observation, but would require an almost complete cessation of output by around 100-150d post BMT, a point at which we could still detect de novo Treg in abundance. In line with this, a simple homogeneous model of naive Treg homeostasis, which took the waning levels of de novo Treg in the thymus as input, still predicted replenishment approaching 90%. Instead, we suggest that the naive Treg pool is homeostatically heterogeneous

at the time of BMT, comprising a subset of Treg with enhanced survival and self renewal properties that confer a competitive advantage over newly generated Treg. The mechanisms resulting in the generation and maintenance of such a subset remain to be determined, but given the rapid expansion of both Treg and conventional pools that occurs in neonatal mice, it is possible that Treg that develop during this window exhibit enhanced homeostatic properties to facilitate the rapid population of the periphery.

Finally, the present study and our previous work provide clues regarding the functional importance of peripheral Treg activation states and dynamics. First, our conclusion here that EM Treg are constitutively generated throughout life by self recognition events, parallels our earlier studies of conventional CD4 memory T cell dynamics. In those studies we showed that $CD4^+$ CM and EM T cells are continuously generated and retained in healthy unchallenged laboratory mice, independently of microbiota and foreign antigenic stimulation (*55, 56, 69*). Continuous generation of these auto-reactive $CD4^+$ memory T cells does not appear to be associated with development of overt autoimmune pathology. We speculate that the tonic generation of EM Treg in parallel with conventional $CD4^+$ memory subsets represents an active and necessary regulatory response and may even share antigenic drivers. Second, we reveal the pathological consequences of maintaining a pool of circulating self-reactive EM Treg. Treg that first infiltrate the TME appear to derive predominantly from circulating EM Treg. While there is much interest in the role of tumor neo-antigens in shaping both conventional and regulatory T cell responses to tumors, the recruitment of primed self-reactive EM Treg to the TME would appear the most teleological solution for tumors to generate the most suppressive environment, since self-antigens likely remain the most abundant source of regulatory T cell stimulation, regardless of tumor evolution and adaptation. An appreciation of the ontogeny of Treg found in TME may be essential if they are to be successfully targeted by immunotherapy without compromising self-tolerance.

Caveats and limitations : Our analysis of Treg antigen specificity inevitably focused on microbial derived antigen. We note however, that germ free mice are not free of foreign antigen, since food antigens may represent a significant source of foreign antigen. We analyzed Treg ontogeny in the TME of transplanted tumors. It will be important to validate our finding in endogenously generated or spontaneous tumor models.

Materials and methods

Study design

The study aimed to quantify the cell dynamics of regulatory T cell subsets across the life course, mapping the fate of different precursors for different subpopulations, and use these approaches to define the ontogeny of Treg that infiltrate the tumor microenvironment following tumor development. WT mice and busulfan bone marrow chimeras were used to define the dynamics of Treg throughout the life course. An inducible Foxp3CreERT fate reporter strain was used to track the fate of Foxp3 expressing cells at a fixed point in time, following a signal treatment with tamoxifen inducer. Mathematical models were used to analyse data from WT mice and chimeras and test different candidate models of naïve and EM Treg homeostasis. This study was not blinded. Both male and female mice were used in the study. Numbers of samples and independent experiments are indicated in the figure legends.

Busulfan Chimeras and Foxp3 reporter strains

Busulfan chimeric C57Bl6/J mice were generated as described in (*70*). In summary, B6.SJL-*Ptprc*^{a} *Pepc*^{b}/BoyJ mice (B6.CD45.1) and C57Bl6/J (B6.CD45.2) mice were bred and maintained in conventional colonies in the Comparative Biology Unit, Royal Free Campus of University College London, or where indicated, at the MRC National Institute for Medical Research, London, UK (NIMR). At NIMR, mice were housed in open cages and fed tap water. At UCL, mice were housed in individually ventilated cages, fed irradiated food and drank irradiated water. Germ Free and matched SPF mice were obtained from the Oxford Centre for Microbiome Studies, Oxford, UK. B6.CD45.1 mice aged between 8 and 25 weeks were treated with 20 mg/kg busulfan (Busilvex, Pierre Fabre) to deplete HSC, and reconstituted with T-cell depleted bone marrow cells from congenic donor B6.CD45.2 mice. Chimeras were sacrificed at various times after bone marrow transplantation. Cervical, brachial, axillary, inguinal and mesenteric lymph nodes, spleen and thymus were dissected from mice; single cell suspensions prepared, and analyzed by flow cytometry.

Foxp3$^{tm9(EGFP/cre/ERT2)Ayr}$/J mice (Jax strain 016961) and B6.Cg-*Gt(ROSA)26Sor*$^{tm9(CAG-tdTomato)Hze}$/J mice (Jax strain 7909, *Rosa26R*^{mTom} hereon) were obtained from Jax Laboratories and interbred to homozygosity at both loci. Mice were fed with tamoxifen by a single feed of 2mg of tamxoxifen (Sigma) diluted in 100μl corn oil (Fisher Scientific).

All experiments were performed in accordance with UK Home Office regulations, project license number PP2330953.

Cell lines and tumor engraftment

MC38 (colon carcinoma), EL4 (T cell lymphoma) and A20 (B cell lymphoma) cell lines were passaged in vitro using standard conditions in DMEM culture media with 10% FCS. MC38 cells were

passaged using 0.5% Trypsin EDTA 1X solution (Gibco). For engraftment into mice, cells were recovered at the exponential phase of growth in vitro, washed and resuspended in tissue culture grade 1X Phosphate Buffer Saline (PBS). Cells were then counted using the CASY counter and injected (5 x 10^6/host) via the s.c. route, near the neck fold of host mice. Body weight and tumor diameter measurements were done at regular intervals. Tumors were permitted to grow up to a maximal diameter of 15mm over a period of 14-20 days. A20 tumors were transplanted into male (male Balb/c x female *Foxp3*$^{EGFP\text{-}CreERT2}$ *Rosa26R*^{mTom})F1 mice.

Flow cytometry and electronic gating strategies

Flow cytometric analysis was performed with 2-5 x 10^6 thymocytes, 1-5 x 10^6 lymph node or spleen cells. Cell concentrations of thymocytes, lymph nodes and spleen cells were determined with a Scharf Instruments Casy Counter. Cells were incubated with saturating concentrations of antibodies in 100 µl of Dulbecco's phosphate-buffered saline (PBS) containing bovine serum albumin (BSA, 0.1%) for 1hour at 4°C followed by two washes in PBS-BSA. Cells were stained with the following monoclonal antibodies and cell dyes: CD45.1 FITC, CD45.2 AlexaFluor 700, TCR-beta APC, CD4 PerCP-eFluor710, CD25 PE, CD44 APC-eFluor780, CD25 eFluor450, CD62L eFluor450 (all eBioscience), TCR-beta PerCP-Cy5.5, CD5 BV510, CD4 BV650, CD44 BV785 (all BioLegend), CD62L BUV737 (BD Biosciences), LIVE/DEAD nearIR and LIVE/DEAD Blue viability dyes (Invitrogen). Foxp3 and Ki67 co-staining was performed using the FITC Flow Kit (BD Biosciences) according to the manufacturer's instructions, along with anti-Ki67 eFluor660 (eBioscience). Cells were acquired on a BD LSR-II or BD 605 LSR-Fortessa flow cytometer and analyzed using Flowjo software (Treestar). Thymic subset gates were as follows: CD4SP: $CD4^+CD8^-TCR\beta^+$. DP: $CD4^+CD8^+$. Naive Treg: live $TCR\beta^+$ $CD4^+CD8^-$ $Foxp3^+$ $CD44^{lo}$ $CD62L^{hi}$. Effector memory Treg: live $TCR\beta^+$ $CD4^+CD8^-$ $Foxp3^+$ $CD44^{hi}$ $CD62L^{lo}$.

Peripheral subset gates were as follows: CD4 naive: live $TCR\beta^+$ $CD4^+$ $Foxp3^-$ $CD44^{lo}$ $CD62L^{hi}$. CD4 TEM: live $TCR\beta^+$ $CD4^+$ $Foxp3^-$ $CD44^{hi}$ $CD62L^{lo}$. CD4 TCM: live $TCR\beta^+$ $CD4^+$ $Foxp3^-$ $CD44^{hi}$ $CD62L^{hi}$. Naive Treg: live $TCR\beta^+$ $CD4^+$ $Foxp3^+$ $CD44^{lo}$ $CD62L^{hi}$. Effector memory Treg: live $TCR\beta^+$ $CD4^+$ $Foxp3^+$ $CD44^{hi}$ $CD62L^{lo}$.

Mathematical modelling and statistical analysis

The mathematical models and our approach to model fitting are detailed in Text S1 of in SI. All code and data used to perform model fitting, and details of the prior distributions for parameters, are available at https:// https://zenodo.org/records/15368583 (DOI 10.5281/zenodo.15368582). Models were ranked using the Leave-One-Out (LOO) cross validation method (*71*). We quantified the relative support for models with the expected log point-wise predictive density (ELPD), for which we report the standard error. Models with ELPD differences below 4 were considered similar.

Statistics

Statistical analysis, line fitting, regression analysis, and figure preparation were performed using Graphpad Prism 8. Column data compared by unpaired Mann-Witney student's t test. * $p<0.05$, ** $p<0.01$, *** $p<0.001$, **** $p < 0.0001$, unless otherwise stated.

Figure 1 - Thymic development of regulatory T cells. Busulfan chimeras were generated using B6.CD45.1 hosts and B6.CD45.2 donors (See Methods) and mice analyzed at various times after BMT. (A) Scatter plot of donor chimerism in DP1 thymocytes of all chimeras analyzed. (B) Gating strategy to identify naive ($CD62L^{hi}CD44^{lo}$) and EM ($CD62L^{lo}CD44^{hi}$) $Foxp3^{+}$ Treg in thymus, and donor (CD45.2) vs host (CD45.1) composition therein. (C) Scatter plots show total number of DP1, CD4 single positive (CD4SP) and Treg (CD4SP $Foxp3^{+}$) subsets isolated from thymus of chimeras (black open) and untreated WT control mice (red diamonds), with mouse age. For linear regression lines, * $p < 0.0001$ that slope is non-zero. (D) Scatter plots of total numbers of naive and EM Treg from chimeras and WT control, by host age. (E) Scatter plots of normalized donor fraction at different times post-BMT amongst CD4SP, naive Treg and EM Treg subsets. Comparison, by non-parametric students T test (* $p < 0.0001$), of donor chimerism amongst CD4SP and naive Treg is for chimeras >42d post BMT. Summary bars show mean and s.d. Data are pooled from five independent batches of chimeras (n=45) and WT controls (n=34).

Figure 2 - Mapping the developmental dynamics of regulatory T cell subsets in busulfan chimeras. Cells from lymph node and spleen from busulfan chimeras and WT mice described in figure 1 were analyzed. (A) Gating strategy to identify naive ($CD62L^{hi}CD44^{lo}$) and EM ($CD62L^{lo}CD44^{hi}$) $Foxp3^{+}$ Treg in peripheral lymphoid organs, their donor (CD45.2) vs host (CD45.1) composition therein, and gates used to measure Ki67 expression. (B-C) Scatter plots are of total numbers of naive (B) and EM (C) Treg recovered from lymph node and spleen of chimeras and control WT mice of different ages. Lines show simple linear regression fits to data. (D) Scatter plot of ratio of naive to EM Treg in lymph node and spleen of WT (filled symbols) and busulfan chimeras (empty symbols) at different host ages. (E) Scatter plots of normalized donor fraction in lymph node and spleen of busulfan chimeras at different times post BMT for naive and EM Treg. (F) Scatter plot showing ratios of donor chimerism in naive (blue) and EM Treg (red) between lymph node : spleen. Panels G-H; The estimated fractions of de novo developed Treg amongst (G) total naive thymic $foxp3^{+}$ cells and (H) total (naive and memory) $Foxp3^{+}$ thymic Treg. (I) De novo generated naive Treg as a fraction of total CD4SP thymocytes. For linear regression lines (B, C, I), * $p < 0.001$ that slope is non-zero.

Figure 3 - Naive Treg are heterogeneous in their homeostatic dynamics. (A) Schematics of the homogeneous and incumbent models of naive Treg homeostasis. (B,C) Best fits of the homogeneous and incumbent models, respectively, to the numbers and normalized donor fraction of naive Treg cells over time. (D,E) The two models' fitted trajectories of Ki67 expression within donor and host cells. Mice were grouped by age at BMT, in weeks; 6-8 (n=10), 8-10 (n=11),

10-12 (n=9) and 12-25 (n=9). (F) Mean residence and interdivision times of naive Treg in the incumbent model, with 95% confidence intervals. (G) The estimated proportion of daily production of naive Treg that derived from self-renewal rather than de novo production. (H) The estimated proportion of Treg that were incumbent (host-derived, established before BMT). Shaded regions indicate 95% confidence envelopes.

Figure 4 - Memory Treg are constitutively replenished from naive Treg and transition from fast to slow turnover following their de novo generation. (A) Schematic of the two-compartment model of memory Treg homeostasis. (B-D) The fitted time courses of the total numbers of memory Treg (B), donor fraction (C), and levels of Ki67 (D) in busulfan chimeric mice, grouped by age at BMT (6-8wks, n=10; 8-10wks, n=11; 10-12wks, n=9; and 12-25wks, n=9). (E) Estimated mean interdivision times and residence times (mean time before death or onward differentiation) of fast and slow memory Treg. (F) Daily proportional influx of fast and slow subsets by newly generated memory.

Figure 5 - Foxp3-FR fate mapping implicates naive Treg as the source of de novo EM Treg. Foxp3-FR mice (n=22) were treated with a single feed of 2mg of tamoxifen and cohorts of mice taken at different times after treatment. (A) Histograms (top row) show mTom reporter expression at the indicated days after treatment by $CD4^+TCR^{hi}$ $Foxp3^+$ cells from lymph nodes. Scatter plots show CD25 vs Foxp3EGFP expression by mTom+ve and mTom-ve $CD4^+$ T cells from lymph nodes. Histograms (bottom row) are of Foxp3-EGFP expression by $mTom^+$ $CD4^+TCR^{hi}$ T cells or total $CD4^+TCR^{hi}$ cells from lymph nodes at different times after treatment. (B-C) Scatter plots are of fraction of naive (B) or EM (C) $Foxp3^+$ Treg that are mTom -ve, calculated from total numbers of Treg recovered from LN and spleen. Splines (long dashes) are best fit lines of normalized donor fractions observed in busulfan chimeras in either naive or EM Treg as shown in figure 2E. A linear regression line with 95% confidence intervals is applied to mTom-ve fraction of memory Treg. Slope deviation from 0, $p = 0.013$. Data are pooled from four independent experiments.

Figure 6 - Tonic memory Treg generation is insensitive to environmental antigens. (A) Treg numbers were measured in spleen from young (70d) or old (145-180d) WT mice maintained in either conventional (n=7 young, n=6 old) SPF or germ free (n=9 young, n=7 old) barrier facilities. Bar charts (left, middle) are of numbers of naive and EM Treg recovered from different aged hosts from different holding facilities, and of Ki67 expression. (B-D) Data from busulfan chimeras detailed in

fig. 1 (grey symbols, clean), generated and analyzed at the UCL Comparative Biology Unit, were compared with chimeras generated in an identical manner three years previously, at the MRC National Institute for Medical Research (red symbols, dirty). In this meta-analysis, Treg were identified by $CD4^+CD25^+$ gate throughout, since earlier study did not include Foxp3 intracellular stain. (B) Ratio of memory:naive $CD4^+$ T_{conv} cells calculated from total numbers of subpopulations recovered from lymph nodes and spleen from different experiments, for central (CM) and effector memory (EM) conventional T cells. Lines are linear regressions to data. (C) Comparison of normalized donor fractions (C) and absolute cell numbers of donors cells (D) for naive and EM Treg in busulfan chimeras generated in dirty and clean environments.

Figure 7 - Intratumoral Treg derive almost exclusively from pre-existing circulating EM Treg. (A-B) Foxp3-FR mice (n=10) were treated with a single feed of tamoxifen and 14 days later, engrafted with MC38 tumor cells. Mice were culled when tumor size reached maximal permitted size (15mm), between 15-20d post engraftment. (A) Density plots show TCR, CD4 and Foxp3 gates used to identify Treg in lymph node (LN) and tumor of host mice, and their naive vs EM composition. (B) Histograms and bar charts show representative and summarized expression of PD1, Ki67 and mTom by naive and EM Treg in LN and spleen, compared with tumor infiltrating Treg. (C) Busulfan chimeras were generated as described in figure 1. Hosts were engrafted with MC38 cells ~8 weeks post BMT. Mice were culled when tumor size reached maximal permitted size, and phenotype of Treg in lymph nodes and tumor determined. Density plot show CD25 vs Foxp3-EGFP, and CD62L vs CD44 used to gate naive and EM phenotype Treg. Plots of CD45.1 and CD45.2 indicate host and donor composition of the indicated Treg subsets, and summary bar charts of normalized donor fraction across all mice (n=9 pooled from three independent experiments). (D) Foxp3FR mice were treated with a single feed of tamoxifen and 14 days later, engrafted with either A20 (n=11) or EL4 (n=6) tumor cells. (Foxp3-FR x Balb/c)F1 mice were used as hosts for A20 tumors. Mice were culled when tumor size reached maximal permitted size and phenotype of Treg assessed as in (B). Data are pool of 5 (B), 3 (C-D) independent experiments.

Supplementary material endnote citations. (*55*) (*58*) (*71*) (*72*)

Supplementary material

S1 Describing precursor influx into naive and EM Tregs

Figure S1: Dynamics of naive Treg precursors

Figure S2: Dynamics of potential precursor populations of EM Tregs

Bibliography

1. A. Saoudi, B. Seddon, V. Heath, D. Fowell, D. Mason, The physiological role of regulatory T cells in the prevention of autoimmunity: the function of the thymus in the generation of the regulatory T cell subset. *Immunol Rev* **149**, 195-216 (1996).
2. Y. Belkaid, K. Tarbell, Regulatory T cells in the control of host-microorganism interactions (*). *Annu Rev Immunol* **27**, 551-589 (2009).
3. M. Panduro, C. Benoist, D. Mathis, Tissue Tregs. *Annu Rev Immunol* **34**, 609-633 (2016).
4. Y. Togashi, K. Shitara, H. Nishikawa, Regulatory T cells in cancer immunosuppression - implications for anticancer therapy. *Nat Rev Clin Oncol* **16**, 356-371 (2019).
5. J. L. McGovern, G. P. Wright, H. J. Stauss, Engineering Specificity and Function of Therapeutic Regulatory T Cells. *Front Immunol* **8**, 1517 (2017).
6. L. Amini, J. Kaeda, E. Fritsche, A. Roemhild, D. Kaiser, P. Reinke, Clinical adoptive regulatory T Cell therapy: State of the art, challenges, and prospective. *Front Cell Dev Biol* **10**, 1081644 (2022).
7. L. S. Peng, Y. Zhuang, Y. Shi, Y. L. Zhao, T. T. Wang, N. Chen, P. Cheng, T. Liu, X. F. Liu, J. Y. Zhang, Q. F. Zuo, X. H. Mao, G. Guo, D. S. Lu, P. W. Yu, Q. M. Zou, Increased tumor-infiltrating CD8(+)Foxp3(+) T lymphocytes are associated with tumor progression in human gastric cancer. *Cancer Immunol Immunother* **61**, 2183-2192 (2012).
8. R. Saleh, E. Elkord, FoxP3(+) T regulatory cells in cancer: Prognostic biomarkers and therapeutic targets. *Cancer Lett* **490**, 174-185 (2020).
9. S. Schnellhardt, J. Hirneth, M. Buttner-Herold, C. Daniel, M. Haderlein, A. Hartmann, R. Fietkau, L. Distel, The Prognostic Value of FoxP3+ Tumour-Infiltrating Lymphocytes in Rectal Cancer Depends on Immune Phenotypes Defined by CD8+ Cytotoxic T Cell Density. *Front Immunol* **13**, 781222 (2022).
10. D. M. Pardoll, The blockade of immune checkpoints in cancer immunotherapy. *Nat Rev Cancer* **12**, 252-264 (2012).
11. A. Ribas, J. D. Wolchok, Cancer immunotherapy using checkpoint blockade. *Science* **359**, 1350-1355 (2018).
12. J. D. Wolchok, Checkpoint blockade: the end of the beginning. *Nat Rev Immunol* **21**, 621 (2021).
13. S. Z. Josefowicz, L. F. Lu, A. Y. Rudensky, Regulatory T cells: mechanisms of differentiation and function. *Annu Rev Immunol* **30**, 531-564 (2012).
14. J. Huehn, A. Hamann, Homing to suppress: address codes for Treg migration. *Trends Immunol* **26**, 632-636 (2005).
15. D. J. Campbell, Control of Regulatory T Cell Migration, Function, and Homeostasis. *J Immunol* **195**, 2507-2513 (2015).
16. A. Liston, D. H. Gray, Homeostatic control of regulatory T cell diversity. *Nat Rev Immunol* **14**, 154-165 (2014).
17. A. Saoudi, B. Seddon, D. Fowell, D. Mason, The thymus contains a high frequency of cells that prevent autoimmune diabetes on transfer into prediabetic recipients. *The Journal of experimental medicine* **184**, 2393-2398 (1996).
18. S. Sakaguchi, Naturally arising CD4+ regulatory t cells for immunologic self-tolerance and negative control of immune responses. *Annu Rev Immunol* **22**, 531-562 (2004).
19. X. Tai, M. Cowan, L. Feigenbaum, A. Singer, CD28 costimulation of developing thymocytes induces Foxp3 expression and regulatory T cell differentiation independently of interleukin 2. *Nat Immunol* **6**, 152-162 (2005).
20. C. W. Lio, C. S. Hsieh, A two-step process for thymic regulatory T cell development. *Immunity* **28**, 100-111 (2008).
21. W. Fu, A. Ergun, T. Lu, J. A. Hill, S. Haxhinasto, M. S. Fassett, R. Gazit, S. Adoro, L. Glimcher, S. Chan, P. Kastner, D. Rossi, J. J. Collins, D. Mathis, C. Benoist, A multiply redundant genetic switch 'locks in' the transcriptional signature of regulatory T cells. *Nat Immunol* **13**, 972-980 (2012).
22. N. Ohkura, M. Hamaguchi, H. Morikawa, K. Sugimura, A. Tanaka, Y. Ito, M. Osaki, Y. Tanaka, R. Yamashita, N. Nakano, J. Huehn, H. J. Fehling, T. Sparwasser, K. Nakai, S.

Sakaguchi, T cell receptor stimulation-induced epigenetic changes and Foxp3 expression are independent and complementary events required for Treg cell development. *Immunity* **37**, 785-799 (2012).
23. X. Tai, B. Erman, A. Alag, J. Mu, M. Kimura, G. Katz, T. Guinter, T. McCaughtry, R. Etzensperger, L. Feigenbaum, D. S. Singer, A. Singer, Foxp3 transcription factor is proapoptotic and lethal to developing regulatory T cells unless counterbalanced by cytokine survival signals. *Immunity* **38**, 1116-1128 (2013).
24. D. Marshall, C. Sinclair, S. Tung, B. Seddon, Differential requirement for IL-2 and IL-15 during bifurcated development of thymic regulatory T cells. *J Immunol* **193**, 5525-5533 (2014).
25. M. Kanamori, H. Nakatsukasa, M. Okada, Q. Lu, A. Yoshimura, Induced Regulatory T Cells: Their Development, Stability, and Applications. *Trends Immunol* **37**, 803-811 (2016).
26. W. Chen, W. Jin, N. Hardegen, K. J. Lei, L. Li, N. Marinos, G. McGrady, S. M. Wahl, Conversion of peripheral CD4+CD25- naive T cells to CD4+CD25+ regulatory T cells by TGF-beta induction of transcription factor Foxp3. *J Exp Med* **198**, 1875-1886 (2003).
27. M. A. Curotto de Lafaille, N. Kutchukhidze, S. Shen, Y. Ding, H. Yee, J. J. Lafaille, Adaptive Foxp3+ regulatory T cell-dependent and -independent control of allergic inflammation. *Immunity* **29**, 114-126 (2008).
28. C. Ohnmacht, J. H. Park, S. Cording, J. B. Wing, K. Atarashi, Y. Obata, V. Gaboriau-Routhiau, R. Marques, S. Dulauroy, M. Fedoseeva, M. Busslinger, N. Cerf-Bensussan, I. G. Boneca, D. Voehringer, K. Hase, K. Honda, S. Sakaguchi, G. Eberl, MUCOSAL IMMUNOLOGY. The microbiota regulates type 2 immunity through RORgammat(+) T cells. *Science* **349**, 989-993 (2015).
29. J. M. Weiss, A. M. Bilate, M. Gobert, Y. Ding, M. A. Curotto de Lafaille, C. N. Parkhurst, H. Xiong, J. Dolpady, A. B. Frey, M. G. Ruocco, Y. Yang, S. Floess, J. Huehn, S. Oh, M. O. Li, R. E. Niec, A. Y. Rudensky, M. L. Dustin, D. R. Littman, J. J. Lafaille, Neuropilin 1 is expressed on thymus-derived natural regulatory T cells, but not mucosa-generated induced Foxp3+ T reg cells. *J Exp Med* **209**, 1723-1742, S1721 (2012).
30. B. H. Yang, S. Hagemann, P. Mamareli, U. Lauer, U. Hoffmann, M. Beckstette, L. Fohse, I. Prinz, J. Pezoldt, S. Suerbaum, T. Sparwasser, A. Hamann, S. Floess, J. Huehn, M. Lochner, Foxp3(+) T cells expressing RORgammat represent a stable regulatory T-cell effector lineage with enhanced suppressive capacity during intestinal inflammation. *Mucosal Immunol* **9**, 444-457 (2016).
31. B. Akagbosu, Z. Tayyebi, G. Shibu, Y. A. Paucar Iza, D. Deep, Y. F. Parisotto, L. Fisher, H. A. Pasolli, V. Thevin, R. Elmentaite, M. Knott, S. Hemmers, L. Jahn, C. Friedrich, J. Verter, Z. M. Wang, M. van den Brink, G. Gasteiger, T. G. P. Grunewald, J. C. Marie, C. Leslie, A. Y. Rudensky, C. C. Brown, Novel antigen-presenting cell imparts T(reg)-dependent tolerance to gut microbiota. *Nature* **610**, 752-760 (2022).
32. R. Kedmi, T. A. Najar, K. R. Mesa, A. Grayson, L. Kroehling, Y. Hao, S. Hao, M. Pokrovskii, M. Xu, J. Talbot, J. Wang, J. Germino, C. A. Lareau, A. T. Satpathy, M. S. Anderson, T. M. Laufer, I. Aifantis, J. M. Bartleson, P. M. Allen, H. Paidassi, J. M. Gardner, M. Stoeckius, D. R. Littman, A RORgammat(+) cell instructs gut microbiota-specific T(reg) cell differentiation. *Nature* **610**, 737-743 (2022).
33. K. Itahashi, T. Irie, H. Nishikawa, Regulatory T-cell development in the tumor microenvironment. *Eur J Immunol* **52**, 1216-1227 (2022).
34. M. Ahmadzadeh, A. Pasetto, L. Jia, D. C. Deniger, S. Stevanovic, P. F. Robbins, S. A. Rosenberg, Tumor-infiltrating human CD4(+) regulatory T cells display a distinct TCR repertoire and exhibit tumor and neoantigen reactivity. *Sci Immunol* **4**, (2019).
35. M. Yadav, C. Louvet, D. Davini, J. M. Gardner, M. Martinez-Llordella, S. Bailey-Bucktrout, B. A. Anthony, F. M. Sverdrup, R. Head, D. J. Kuster, P. Ruminski, D. Weiss, D. Von Schack, J. A. Bluestone, Neuropilin-1 distinguishes natural and inducible regulatory T cells among regulatory T cell subsets in vivo. *J Exp Med* **209**, 1713-1722, S1711-1719 (2012).
36. A. M. Thornton, P. E. Korty, D. Q. Tran, E. A. Wohlfert, P. E. Murray, Y. Belkaid, E. M. Shevach, Expression of Helios, an Ikaros transcription factor family member, differentiates thymic-derived from peripherally induced Foxp3+ T regulatory cells. *J Immunol* **184**, 3433-3441 (2010).

37. E. Szurek, A. Cebula, L. Wojciech, M. Pietrzak, G. Rempala, P. Kisielow, L. Ignatowicz, Differences in Expression Level of Helios and Neuropilin-1 Do Not Distinguish Thymus-Derived from Extrathymically-Induced CD4+Foxp3+ Regulatory T Cells. *PLoS One* **10**, e0141161 (2015).
38. E. Elkord, Helios Should Not Be Cited as a Marker of Human Thymus-Derived Tregs. Commentary: Helios(+) and Helios(-) Cells Coexist within the Natural FOXP3(+) T Regulatory Cell Subset in Humans. *Front Immunol* **7**, 276 (2016).
39. S. Fisson, G. Darrasse-Jeze, E. Litvinova, F. Septier, D. Klatzmann, R. Liblau, B. L. Salomon, Continuous activation of autoreactive CD4+ CD25+ regulatory T cells in the steady state. *J Exp Med* **198**, 737-746 (2003).
40. J. Huehn, K. Siegmund, J. C. Lehmann, C. Siewert, U. Haubold, M. Feuerer, G. F. Debes, J. Lauber, O. Frey, G. K. Przybylski, U. Niesner, M. de la Rosa, C. A. Schmidt, R. Brauer, J. Buer, A. Scheffold, A. Hamann, Developmental stage, phenotype, and migration distinguish naive- and effector/memory-like CD4+ regulatory T cells. *J Exp Med* **199**, 303-313 (2004).
41. G. L. Stephens, J. Andersson, E. M. Shevach, Distinct subsets of FoxP3+ regulatory T cells participate in the control of immune responses. *J Immunol* **178**, 6901-6911 (2007).
42. M. Feuerer, J. A. Hill, D. Mathis, C. Benoist, Foxp3+ regulatory T cells: differentiation, specification, subphenotypes. *Nat Immunol* **10**, 689-695 (2009).
43. D. J. Campbell, M. A. Koch, Phenotypical and functional specialization of FOXP3+ regulatory T cells. *Nat Rev Immunol* **11**, 119-130 (2011).
44. M. Xu, M. Pokrovskii, Y. Ding, R. Yi, C. Au, O. J. Harrison, C. Galan, Y. Belkaid, R. Bonneau, D. R. Littman, c-MAF-dependent regulatory T cells mediate immunological tolerance to a gut pathobiont. *Nature* **554**, 373-377 (2018).
45. M. A. Koch, G. Tucker-Heard, N. R. Perdue, J. R. Killebrew, K. B. Urdahl, D. J. Campbell, The transcription factor T-bet controls regulatory T cell homeostasis and function during type 1 inflammation. *Nat Immunol* **10**, 595-602 (2009).
46. F. Yu, S. Sharma, J. Edwards, L. Feigenbaum, J. Zhu, Dynamic expression of transcription factors T-bet and GATA-3 by regulatory T cells maintains immunotolerance. *Nat Immunol* **16**, 197-206 (2015).
47. Y. Chung, S. Tanaka, F. Chu, R. I. Nurieva, G. J. Martinez, S. Rawal, Y. H. Wang, H. Lim, J. M. Reynolds, X. H. Zhou, H. M. Fan, Z. M. Liu, S. S. Neelapu, C. Dong, Follicular regulatory T cells expressing Foxp3 and Bcl-6 suppress germinal center reactions. *Nat Med* **17**, 983-988 (2011).
48. J. A. Pai, M. D. Hellmann, J. L. Sauter, M. Mattar, H. Rizvi, H. J. Woo, N. Shah, E. M. Nguyen, F. Z. Uddin, A. Quintanal-Villalonga, J. M. Chan, P. Manoj, V. Allaj, M. K. Baine, U. K. Bhanot, M. Jain, I. Linkov, F. Meng, D. Brown, J. E. Chaft, A. J. Plodkowski, M. Gigoux, H. H. Won, T. Sen, D. K. Wells, M. T. A. Donoghue, E. de Stanchina, J. D. Wolchok, B. Loomis, T. Merghoub, C. M. Rudin, A. Chow, A. T. Satpathy, Lineage tracing reveals clonal progenitors and long-term persistence of tumor-specific T cells during immune checkpoint blockade. *Cancer Cell* **41**, 776-790 e777 (2023).
49. B. Seddon, A. J. Yates, The natural history of naive T cells from birth to maturity. *Immunol Rev* **285**, 218-232 (2018).
50. N. Thiault, J. Darrigues, V. Adoue, M. Gros, B. Binet, C. Perals, B. Leobon, N. Fazilleau, O. P. Joffre, E. A. Robey, J. P. van Meerwijk, P. Romagnoli, Peripheral regulatory T lymphocytes recirculating to the thymus suppress the development of their precursors. *Nat Immunol* **16**, 628-634 (2015).
51. J. E. Cowan, N. I. McCarthy, G. Anderson, CCR7 Controls Thymus Recirculation, but Not Production and Emigration, of Foxp3(+) T Cells. *Cell Rep* **14**, 1041-1048 (2016).
52. K. Attridge, L. S. Walker, Homeostasis and function of regulatory T cells (Tregs) in vivo: lessons from TCR-transgenic Tregs. *Immunol Rev* **259**, 23-39 (2014).
53. E. M. van Leeuwen, J. Sprent, C. D. Surh, Generation and maintenance of memory CD4(+) T Cells. *Curr Opin Immunol* **21**, 167-172 (2009).
54. T. Hogan, G. Gossel, A. J. Yates, B. Seddon, Temporal fate mapping reveals age-linked heterogeneity in naive T lymphocytes in mice. *Proc Natl Acad Sci U S A* **112**, E6917-6926 (2015).

55. G. Gossel, T. Hogan, D. Cownden, B. Seddon, A. J. Yates, Memory CD4 T cell subsets are kinetically heterogeneous and replenished from naive T cells at high levels. *Elife* **6**, (2017).
56. T. Hogan, M. Nowicka, D. Cownden, C. F. Pearson, A. J. Yates, B. Seddon, Differential impact of self and environmental antigens on the ontogeny and maintenance of CD4(+) T cell memory. *Elife* **8**, (2019).
57. S. Rane, T. Hogan, E. Lee, B. Seddon, A. J. Yates, Towards a unified model of naive T cell dynamics across the lifespan. *Elife* **11**, e78168 (2022).
58. M. Verheijen, S. Rane, C. Pearson, A. J. Yates, B. Seddon, Fate Mapping Quantifies the Dynamics of B Cell Development and Activation throughout Life. *Cell Rep* **33**, 108376 (2020).
59. T. Boehm, J. B. Swann, Thymus involution and regeneration: two sides of the same coin? *Nat Rev Immunol* **13**, 831-838 (2013).
60. S. Rane, T. Hogan, B. Seddon, A. J. Yates, Age is not just a number: Naive T cells increase their ability to persist in the circulation over time. *PLoS Biol* **16**, e2003949 (2018).
61. Y. P. Rubtsov, R. E. Niec, S. Josefowicz, L. Li, J. Darce, D. Mathis, C. Benoist, A. Y. Rudensky, Stability of the regulatory T cell lineage in vivo. *Science* **329**, 1667-1671 (2010).
62. S. P. Rosshart, J. Herz, B. G. Vassallo, A. Hunter, M. K. Wall, J. H. Badger, J. A. McCulloch, D. G. Anastasakis, A. A. Sarshad, I. Leonardi, N. Collins, J. A. Blatter, S. J. Han, S. Tamoutounour, S. Potapova, M. B. Foster St Claire, W. Yuan, S. K. Sen, M. S. Dreier, B. Hild, M. Hafner, D. Wang, I. D. Iliev, Y. Belkaid, G. Trinchieri, B. Rehermann, Laboratory mice born to wild mice have natural microbiota and model human immune responses. *Science* **365**, (2019).
63. L. K. Beura, S. E. Hamilton, K. Bi, J. M. Schenkel, O. A. Odumade, K. A. Casey, E. A. Thompson, K. A. Fraser, P. C. Rosato, A. Filali-Mouhim, R. P. Sekaly, M. K. Jenkins, V. Vezys, W. N. Haining, S. C. Jameson, D. Masopust, Normalizing the environment recapitulates adult human immune traits in laboratory mice. *Nature* **532**, 512-516 (2016).
64. P. A. Savage, D. S. Leventhal, S. Malchow, Shaping the repertoire of tumor-infiltrating effector and regulatory T cells. *Immunol Rev* **259**, 245-258 (2014).
65. P. Peterson, T. Org, A. Rebane, Transcriptional regulation by AIRE: molecular mechanisms of central tolerance. *Nat Rev Immunol* **8**, 948-957 (2008).
66. T. Yamano, J. Dobes, M. Voboril, M. Steinert, T. Brabec, N. Zietara, M. Dobesova, C. Ohnmacht, M. Laan, P. Peterson, V. Benes, R. Sedlacek, R. Hanayama, M. Kolar, L. Klein, D. Filipp, Aire-expressing ILC3-like cells in the lymph node display potent APC features. *J Exp Med* **216**, 1027-1037 (2019).
67. Z. Liang, X. Dong, Z. Zhang, Q. Zhang, Y. Zhao, Age-related thymic involution: Mechanisms and functional impact. *Aging Cell* **21**, e13671 (2022).
68. J. E. Cowan, S. M. Parnell, K. Nakamura, J. H. Caamano, P. J. Lane, E. J. Jenkinson, W. E. Jenkinson, G. Anderson, The thymic medulla is required for Foxp3+ regulatory but not conventional CD4+ thymocyte development. *J Exp Med* **210**, 675-681 (2013).
69. M. E. Bullock, T. Hogan, C. Williams, S. Morris, M. Nowicka, M. Sharjeel, C. van Dorp, A. J. Yates, B. Seddon, The dynamics and longevity of circulating CD4+ memory T cells depend on cell age and not the chronological age of the host. *PLoS Biol* **22**, e3002380 (2024).
70. T. Hogan, A. Yates, B. Seddon, Generation of Busulfan Chimeric Mice for the Analysis of T Cell Population Dynamics. *Bio Protoc* **7**, e2650 (2017).
71. A. Vehtari, A. Gelman, J. Gabry, Practical Bayesian model evaluation using leave-one-out cross-validation and WAIC. *Statistics and Computing* **27**, 1413-1432 (2017).
72. Y. Yao, A. Vehtari, D. Simpson, A. Gelman, Using Stacking to Average Bayesian Predictive Distributions (with Discussion). *Bayesian Analysis* **13**, 917-1007, 1091 (2018).

Acknowledgements : We thank UCL Comparative Biology Unit staff for assistance with mouse breeding and maintenance.

Data and materials availability: Data used to perform model fitting, and details of the prior distributions for parameters, are available at https:// https://zenodo.org/records/15368583.

Funding: BS and AJY were supported by the National Institutes of Health (R01 AI093870, U01 AI150680). SP was supported by a postdoctoral fellowship funded by AstroZeneca.

Author contribution:

S.P. Designed and performed experiment, analyzed data.

T.H. Designed and performed experiments.

S.R. Designed models, analyzed data, wrote the paper.

Y.H. Performed experiments

C.P. Performed experiments

C.S. Designed experiments and provided funding.

S.B. Provided funding.

L.C. Designed experiments and provided funding.

A.Y. Designed experiments, analyzed data, wrote the paper.

B.S. Designed experiments, analyzed data, wrote the paper

Competing interests: no competing financial interests

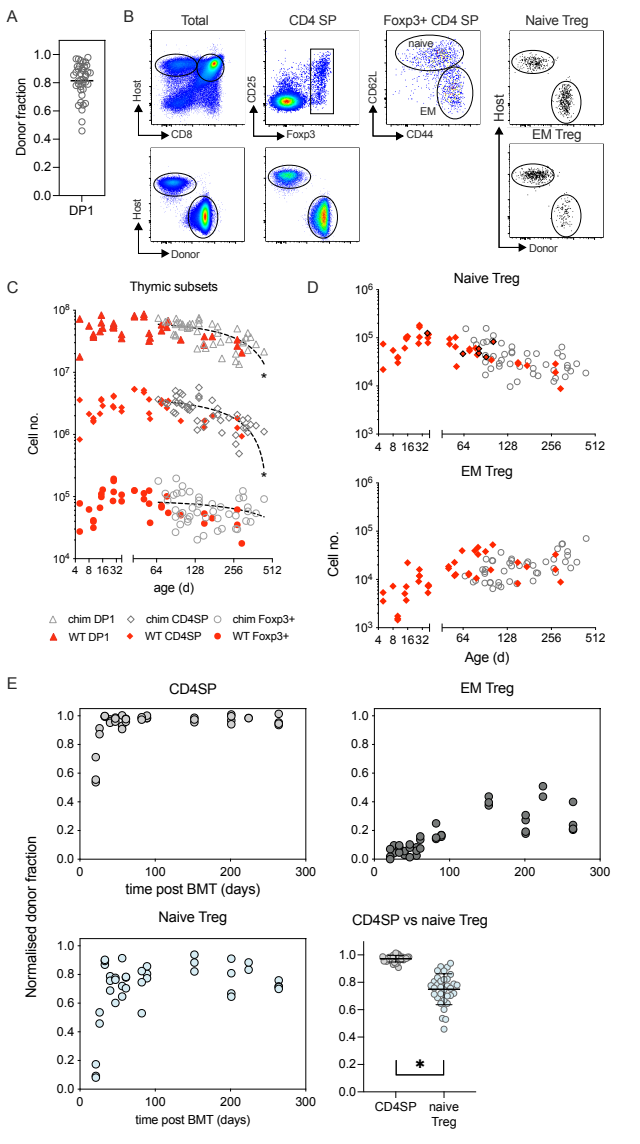
A
Donor fraction
1.0
0.8
0.6
0.4
0.2
0.0
DP1
B
Total
CD4 SP
Foxp3+ CD4 SP
Naive Treg
Host
CD8
CD25
Foxp3
CD62L
CD44
naive
EM
Host
Donor
EM Treg
C
Thymic subsets
Cell no.
age (d)
chim DP1
WT DP1
chim CD4SP
WT CD4SP
chim Foxp3+
WT Foxp3+
D
Naive Treg
EM Treg
Cell no.
Age (d)
E
CD4SP
EM Treg
Normalised donor fraction
time post BMT (days)
Naive Treg
CD4SP vs naive Treg
CD4SP
naive Treg

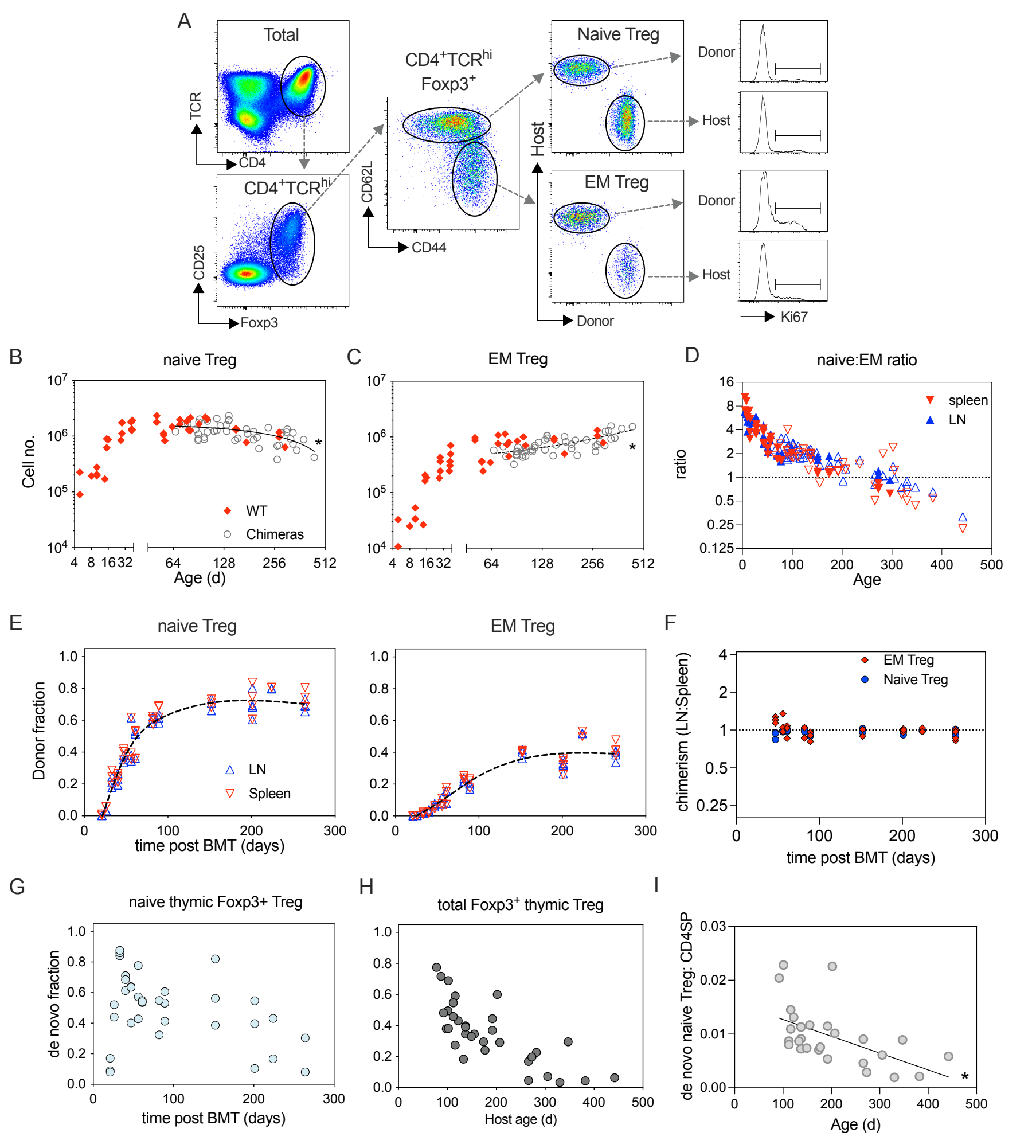
A
Total
TCR
CD4
CD4+TCRhi
CD25
Foxp3
CD4+TCRhi
Foxp3+
CD62L
CD44
Naive Treg
EM Treg
Host
Donor
Donor
Host
Donor
Host
Ki67
B
naive Treg
Cell no.
WT
Chimeras
Age (d)
C
EM Treg
D
naive:EM ratio
ratio
spleen
LN
Age
E
naive Treg
EM Treg
Donor fraction
LN
Spleen
time post BMT (days)
F
chimerism (LN:Spleen)
EM Treg
Naive Treg
time post BMT (days)
G
naive thymic Foxp3+ Treg
de novo fraction
time post BMT (days)
H
total Foxp3+ thymic Treg
Host age (d)
I
de novo naive Treg: CD4SP
Age (d)

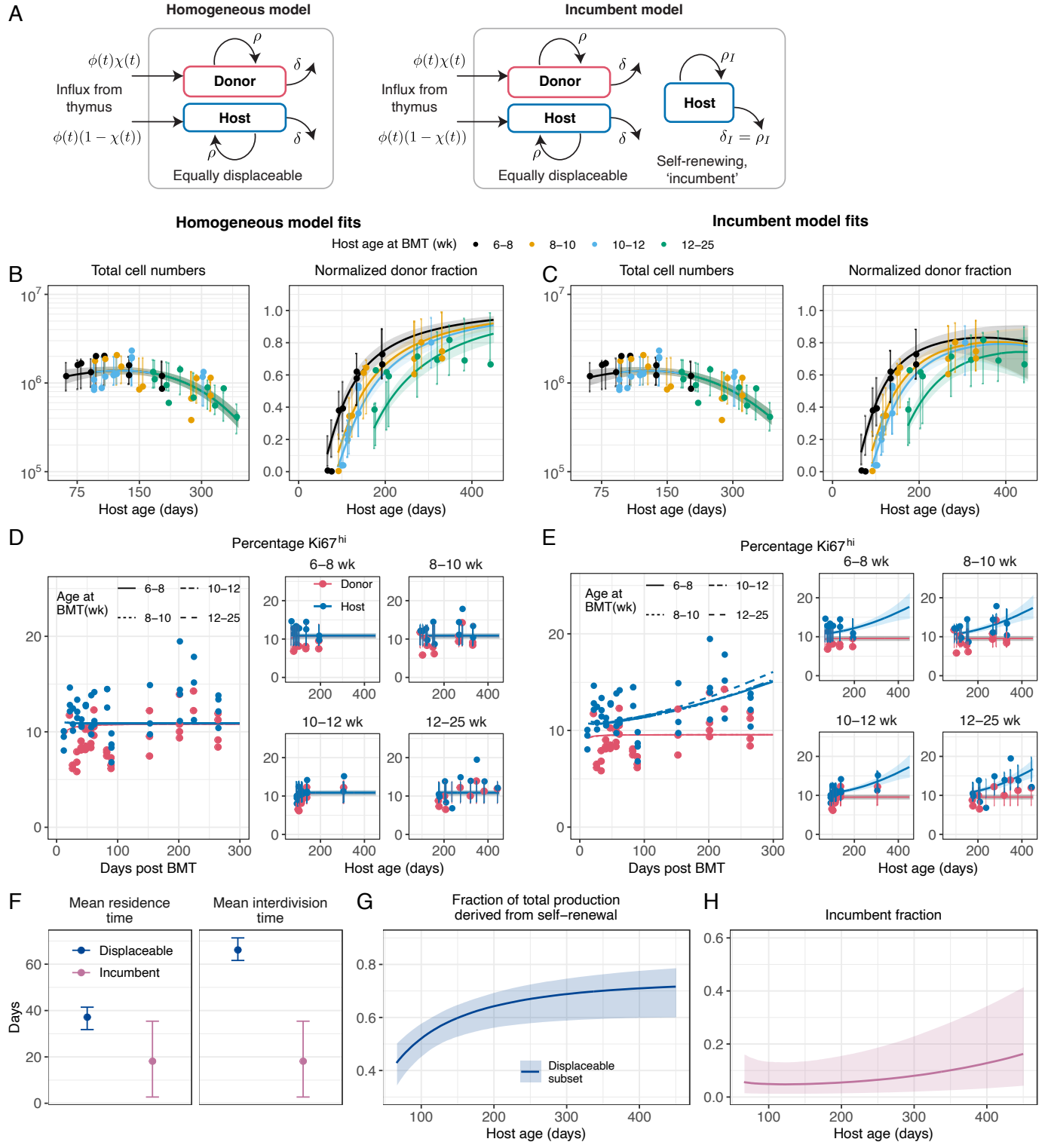
A
Homogeneous model
$\phi(t)\chi(t)$
Influx from thymus
$\phi(t)(1-\chi(t))$
Donor
Host
ρ
δ
Equally displaceable
Incumbent model
Self-renewing, 'incumbent'
ρ_I
$\delta_I = \rho_I$
Homogeneous model fits
Incumbent model fits
Host age at BMT (wk) 6–8 8–10 10–12 12–25
B
C
Total cell numbers
Normalized donor fraction
Host age (days)
D
E
Percentage Ki67hi
Age at BMT(wk)
6–8 wk
8–10 wk
10–12 wk
12–25 wk
Days post BMT
F
Mean residence time
Mean interdivision time
Displaceable
Incumbent
Days
G
Fraction of total production derived from self–renewal
Displaceable subset
H
Incumbent fraction

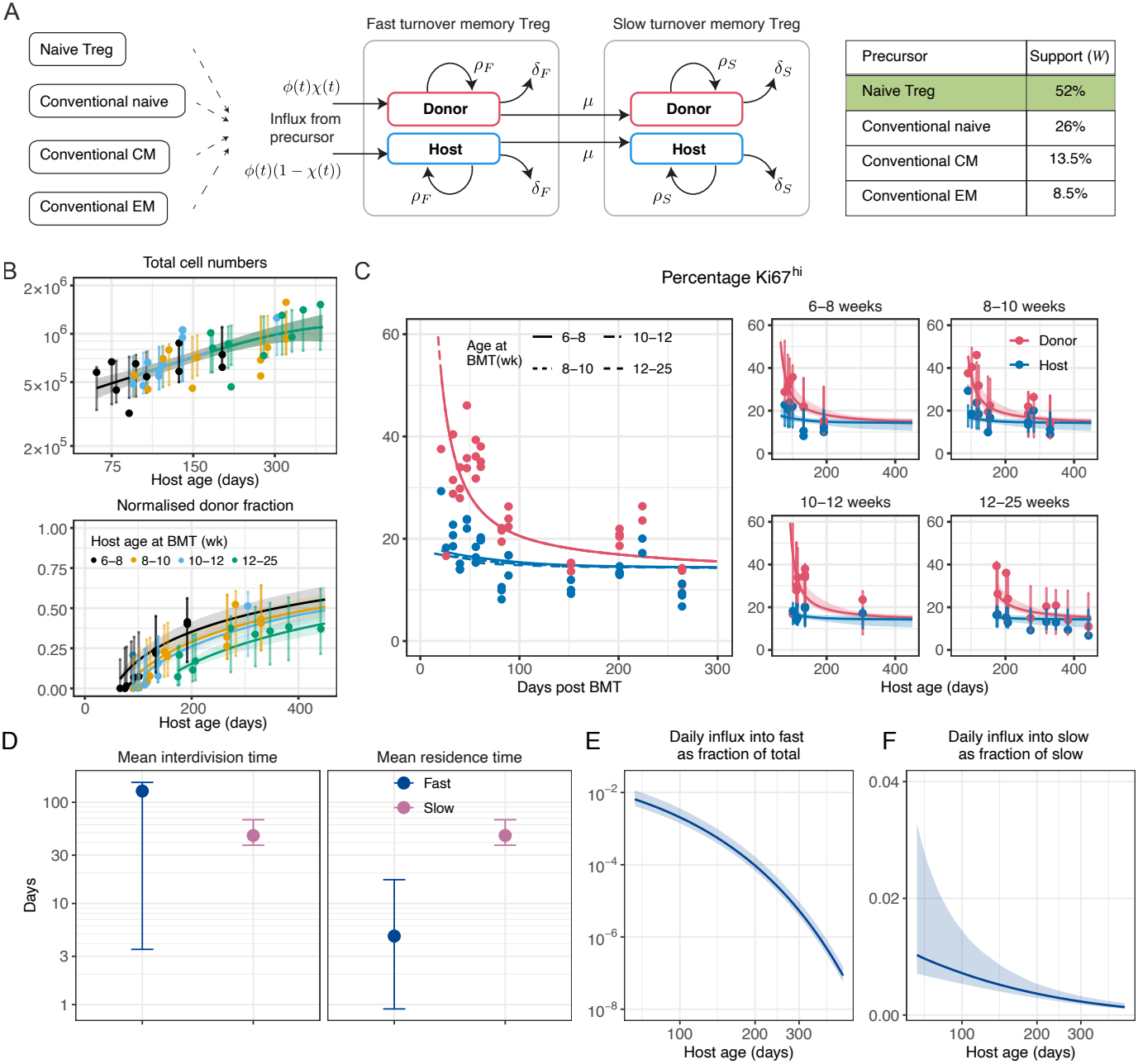
A
Naive Treg
Conventional naive
Conventional CM
Conventional EM
$\phi(t)\chi(t)$
Influx from precursor
$\phi(t)(1-\chi(t))$
Fast turnover memory Treg
Donor
Host
ρ_F
δ_F
μ
Slow turnover memory Treg
ρ_S
δ_S
Precursor | Support (W)
Naive Treg | 52%
Conventional naive | 26%
Conventional CM | 13.5%
Conventional EM | 8.5%
B
Total cell numbers
Host age (days)
Normalised donor fraction
Host age at BMT (wk)
6–8 8–10 10–12 12–25
C
Percentage Ki67^{hi}
Age at BMT(wk)
6–8 10–12 8–10 12–25
Days post BMT
6–8 weeks
8–10 weeks
10–12 weeks
12–25 weeks
Donor
Host
D
Mean interdivision time
Mean residence time
Fast
Slow
Days
E
Daily influx into fast as fraction of total
F
Daily influx into slow as fraction of slow

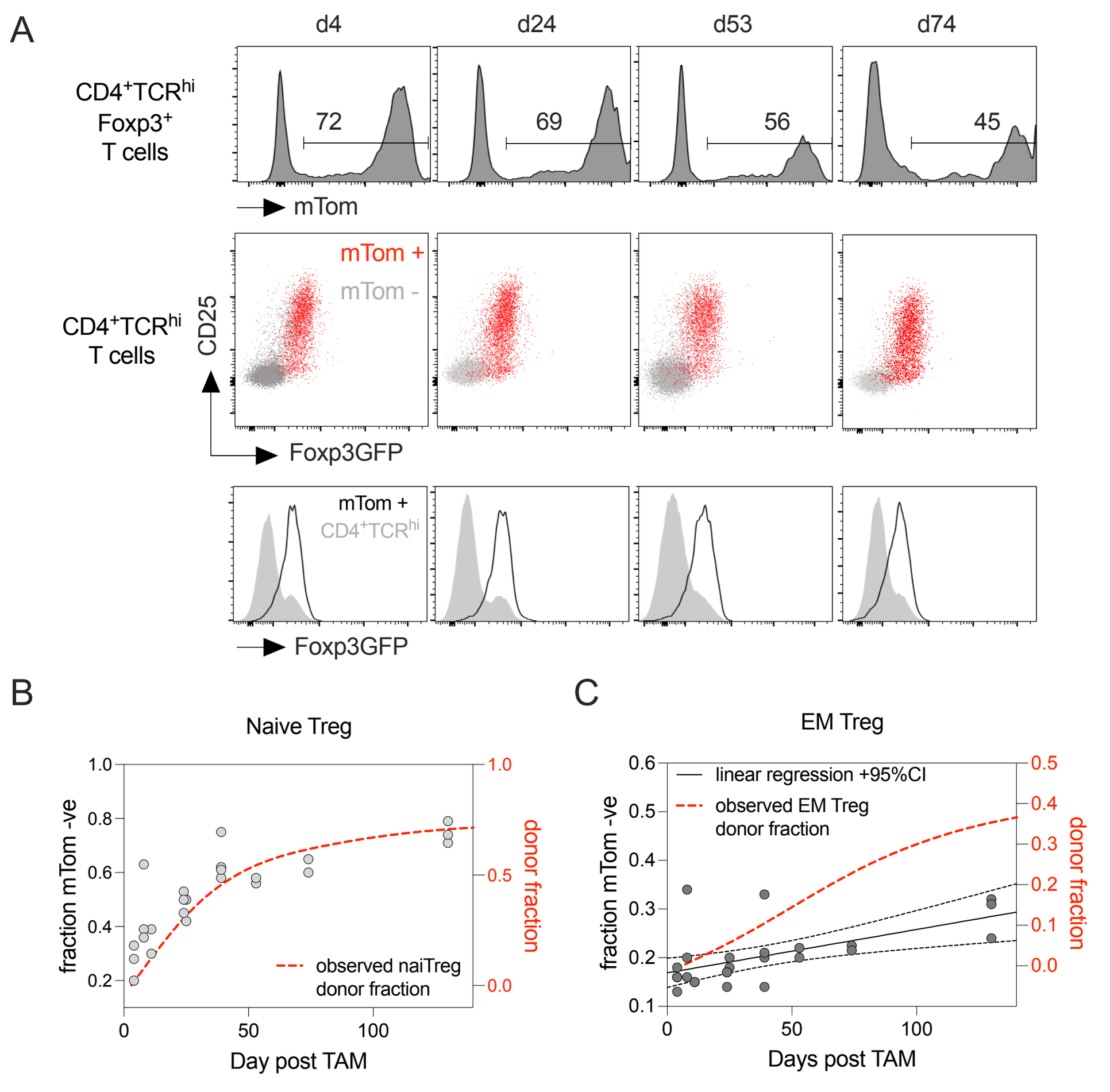
A
d4
d24
d53
d74
CD4+TCRhi Foxp3+ T cells
72
69
56
45
mTom
CD4+TCRhi T cells
CD25
mTom +
mTom -
Foxp3GFP
mTom +
CD4+TCRhi
Foxp3GFP
B
Naive Treg
fraction mTom -ve
donor fraction
observed naiTreg donor fraction
Day post TAM
C
EM Treg
linear regression +95%CI
observed EM Treg donor fraction
fraction mTom -ve
donor fraction
Days post TAM

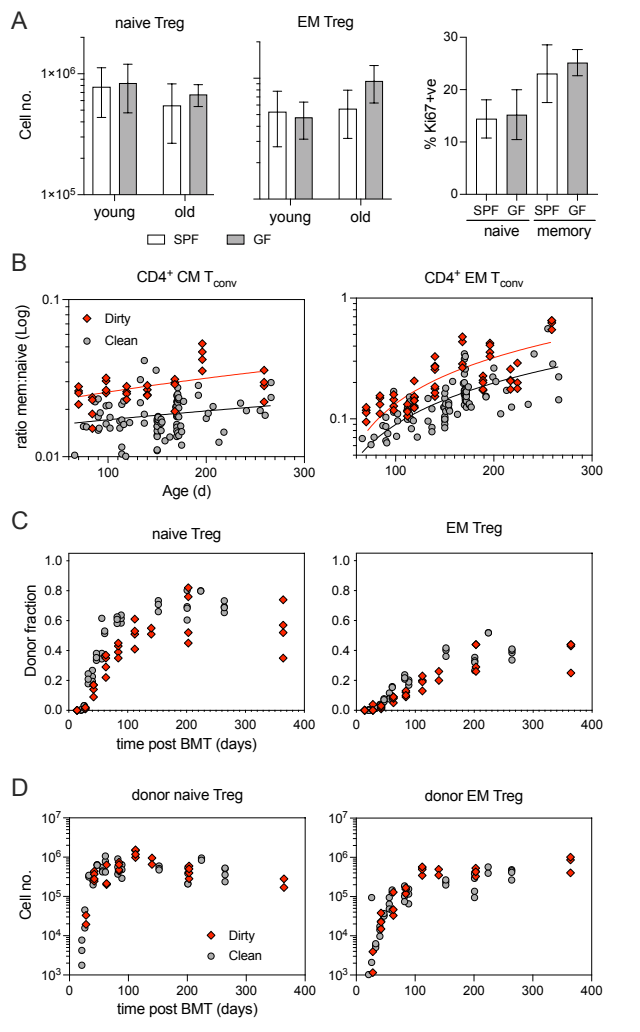
A
naive Treg
EM Treg
Cell no.
1×10^6
1×10^5
young
old
young
old
SPF
GF
% Ki67+ve
30
20
10
0
SPF GF SPF GF
naive
memory
B
CD4+ CM Tconv
CD4+ EM Tconv
ratio mem:naive (Log)
0.1
0.01
Dirty
Clean
100
200
300
Age (d)
1
0.1
C
naive Treg
EM Treg
Donor fraction
1.0
0.8
0.6
0.4
0.2
0.0
0
100
200
300
400
time post BMT (days)
D
donor naive Treg
donor EM Treg
Cell no.
10^7
10^6
10^5
10^4
10^3
Dirty
Clean
time post BMT (days)

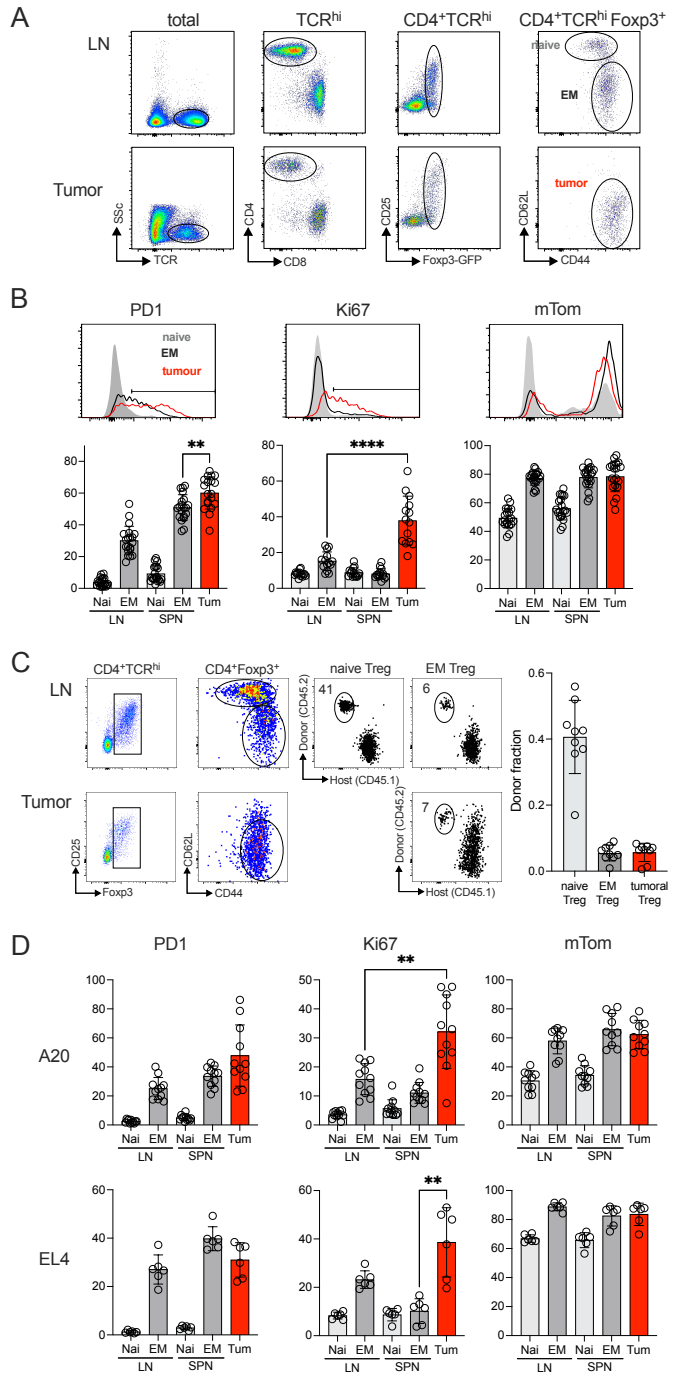
A
total
TCRhi
CD4+TCRhi
CD4+TCRhi Foxp3+
LN
Tumor
naive
EM
tumor
SSc
TCR
CD4
CD8
CD25
Foxp3-GFP
CD62L
CD44
B
PD1
Ki67
mTom
naive
EM
tumour
**
****
Nai EM Nai EM Tum
LN SPN
C
CD4+TCRhi
CD4+Foxp3+
naive Treg
EM Treg
LN
Tumor
41
6
7
Donor (CD45.2)
Host (CD45.1)
CD25
Foxp3
CD62L
CD44
Donor fraction
naive Treg
EM Treg
tumoral Treg
D
PD1
Ki67
mTom
A20
EL4
**
Nai EM Nai EM Tum
LN SPN

S1 Mathematical modeling

S1A Models of naive Treg homeostasis

We modeled the dynamics of naive Tregs in busulfan chimeric mice – the changes in their pool size, their donor:host composition and the extent of their Ki67 expression – using a mechanistic modeling approach. First, we considered a simple **homogeneous model**, which assumes that the birth, death, and maturation dynamics of naive Tregs are governed by processes that remain unchanged over the mouse's lifetime. This model can only explain the incomplete replacement (*i.e.,* normalised chimerism stabilizing to values < 1) in naive Tregs that we observe when the influx of precursor-derived cells declines with time and drops below their net loss rate. That is, the supply of donor-derived cells from their precursors dries up before their donor fraction can equilibrate with the chimerism in their ancestors in the thymus – the early stage CD4 CD8 double positive (DP) thymocytes.

Alternatively, the partial replacement of host cells by donor-derived cells in naive Tregs can also be explained by models assuming heterogeneity in their maintenance. To address this, we included the **incumbent model** in our analyses, which compartmentalizes naive Treg population into two subsets with distinct kinetics birth and loss. Specifically, it defines an 'incumbent' subset composed of self-renewing, long-lived subpopulation of relatively older cells that are established early on in life – before the bone marrow transplant – which are resistant to replacement by newly derived donor cells. The incumbent model also considers a 'displaceable' subset within naive Tregs consisting cells with comparatively rapid kinetics of division and loss. For the purposes of modeling naive Treg dynamics in adult (7 weeks and older) busulfan chimeric mice, we consider that thymic precursors of naive Tregs exclusively feed into the displaceable subset.

General formulations of the neutral and incumbent models

We defined both of these models as the systems of ordinary differential equations (ODE), to separately track the dynamics of incumbent and displaceable compartments in Ki67$^+$ and Ki67$^-$ subsets of donor- and host-derived naive Treg cells.

Neutral model:

Host compartment in busulfan chimeras

Ki67$^+$subset

$$\frac{dX_{\mathsf{h}}^{+}}{dt} = \alpha\,\phi(t)\,(1-\chi(t))\,\epsilon_h + \rho_{\mathsf{x}}\,(2\,X_{\mathsf{h}}^{-} + X_{\mathsf{h}}^{+}) - (\beta+\delta_{\mathsf{x}})\,X_{\mathsf{h}}^{+}$$

Ki67$^-$subset

$$\frac{dX_{\mathsf{h}}^{-}}{dt} = \alpha\,\phi(t)\,(1-\chi(t))\,(1-\epsilon_h) + \beta\,X_{\mathsf{h}}^{+} - (\rho_{\mathsf{x}}+\delta_{\mathsf{x}})\,X_{\mathsf{h}}^{+}$$

Donor compartment in busulfan chimeras

Ki67$^+$subset

$$\frac{dX_{\mathsf{d}}^{+}}{dt} = \alpha\,\phi(t)\,\chi(t)\,\epsilon_d + \rho_{\mathsf{x}}\,(2\,X_{\mathsf{d}}^{-} + X_{\mathsf{d}}^{+}) - (\beta+\delta_{\mathsf{x}})\,X_{\mathsf{d}}^{+}$$

Ki67$^-$subset

$$\frac{dX_{\mathsf{d}}^{-}}{dt} = \alpha\,\phi(t)\,\chi(t)\,(1-\epsilon_d) + \beta\,X_{\mathsf{d}}^{+} - (\rho_{\mathsf{x}}+\delta_{\mathsf{x}})\,X_{\mathsf{d}}^{+}$$

(1)

We used empirical descriptions of the total size of the immediate precursors of naive Tregs and the extent of donor chimerism and fraction of Ki67$^+$ cells within the precursors to define $\phi(t), \chi(t)$ and $\epsilon(t)$. These descriptor functions are explained in detail in the **section S1C**. Both the neutral (equation 1) and the incumbent (equation 2) model estimate the rate of daily influx (α) into naive Tregs, their division and loss rates (ρ and δ) using the data from the busulfan chimeras. Lastly, we used our previous estimate of the rate of loss of Ki67 expression (β) on T cells (Gossel et al eLIfe) and fixed it to $1/3.5$ days^{-1}. We depict the general formulation of the incumbent model similarly below.

Incumbent model:

Host compartment in busulfan chimeras

Displaceable Ki67$^+$subset

$$\frac{dX_{\mathsf{h}}^{+}}{dt} = \alpha\,\phi(t)\,(1-\chi(t))\,\epsilon(t) + \rho_{\mathsf{x}}\,(2\,X_{\mathsf{h}}^{-} + X_{\mathsf{h}}^{+}) - (\beta+\delta_{\mathsf{x}})\,X_{\mathsf{h}}^{+}$$

Displaceable Ki67$^-$subset

$$\frac{dX_{\mathsf{h}}^{-}}{dt} = \alpha\,\phi(t)\,(1-\chi(t))\,(1-\epsilon(t)) + \beta\,X_{\mathsf{h}}^{+} - (\rho_{\mathsf{x}}+\delta_{\mathsf{x}})\,X_{\mathsf{h}}^{+}$$

Incumbent Ki67$^+$subset

$$\frac{dY_{\mathsf{h}}^{+}}{dt} = \rho_{\mathsf{y}}\,(2\,Y_{\mathsf{h}}^{-} + Y_{\mathsf{h}}^{+}) - (\beta+\delta_{\mathsf{y}})\,Y_{\mathsf{h}}^{+}$$

Incumbent Ki67$^-$subset

$$\frac{dY_{\mathsf{h}}^{-}}{dt} = \beta\,Y_{\mathsf{h}}^{+} - (\rho_{\mathsf{y}}+\delta_{\mathsf{y}})\,Y_{\mathsf{h}}^{+}$$

(2)

Donor compartment in busulfan chimeras

Displaceable Ki67$^+$subset

$$\frac{dX_{\mathsf{d}}^{+}}{dt} = \alpha\,\phi(t)\,\chi(t)\,\epsilon(t) + \rho_{\mathsf{x}}\,(2\,X_{\mathsf{d}}^{-} + X_{\mathsf{d}}^{+}) - (\beta+\delta_{\mathsf{x}})\,X_{\mathsf{d}}^{+}$$

Displaceable Ki67$^-$subset

$$\frac{dX_{\mathsf{d}}^{-}}{dt} = \alpha\,\phi(t)\,\chi(t)\,(1-\epsilon(t)) + \beta\,X_{\mathsf{d}}^{+} - (\rho_{\mathsf{x}}+\delta_{\mathsf{x}})\,X_{\mathsf{d}}^{+}$$

Incumbent Ki67$^+$subset

$$\frac{dY_{\mathsf{d}}^{+}}{dt} = \rho_{\mathsf{y}}\,(2\,Y_{\mathsf{d}}^{-} + Y_{\mathsf{d}}^{+}) - (\beta+\delta_{\mathsf{y}})\,Y_{\mathsf{d}}^{+}$$

Incumbent Ki67$^-$subset

$$\frac{dY_{\mathsf{d}}^{-}}{dt} = \beta\,Y_{\mathsf{d}}^{+} - (\rho_{\mathsf{y}}+\delta_{\mathsf{y}})\,Y_{\mathsf{d}}^{+}$$

S1B Modeling EM Treg dynamics

We used a two-compartmental model that encodes heterogeneity in EM Treg turnover to explain their behaviour in busulfan chimeric mice. We argued that activation and cell-division events accompany differentiation to the EM Treg lineage, and therefore designed a model that divides cells into two kinetically distinct subsets based on the time since their compartmental entry. In this **two-compartment** model, we considered that new precursor-derived cells enter EM Treg compartment via a 'fast' subset with relatively rapid dynamics of division and death. Cells in the fast before transitioning into a more quiescent 'slow' state.

ODE system depicting the two-compartment model:

Host compartment in busulfan chimeras

Fast Ki67^{+}subset

$$\frac{dX_{\mathsf{h}}^{+}}{dt} = \alpha\,\phi(t)\,(1-\chi(t)) + \rho_{\mathsf{x}}\,(2\,X_{\mathsf{h}}^{-} + X_{\mathsf{h}}^{+}) - (\beta + \delta_{\mathsf{x}} + \mu)\,X_{\mathsf{h}}^{+}$$

Fast Ki67^{-}subset

$$\frac{dX_{\mathsf{h}}^{-}}{dt} = \beta\,X_{\mathsf{h}}^{+} - (\rho_{\mathsf{x}} + \delta_{\mathsf{x}} + \mu)\,X_{\mathsf{h}}^{+}$$

Slow Ki67^{+}subset

$$\frac{dY_{\mathsf{h}}^{+}}{dt} = \mu\,X_{\mathsf{h}}^{+} + \rho_{\mathsf{y}}\,(2\,Y_{\mathsf{h}}^{-} + Y_{\mathsf{h}}^{+}) - (\beta + \delta_{\mathsf{y}})\,Y_{\mathsf{h}}^{+}$$

Slow Ki67^{-}subset

$$\frac{dY_{\mathsf{h}}^{-}}{dt} = \mu X_{\mathsf{h}}^{+} + \beta\,Y_{\mathsf{h}}^{+} - (\rho_{\mathsf{y}} + \delta_{\mathsf{y}})\,Y_{\mathsf{h}}^{+}$$

(3)

Donor compartment in busulfan chimeras

Fast Ki67^{+}subset

$$\frac{dX_{\mathsf{d}}^{+}}{dt} = \alpha\,\phi(t)\,(1-\chi(t)) + \rho_{\mathsf{x}}\,(2\,X_{\mathsf{d}}^{-} + X_{\mathsf{d}}^{+}) - (\beta + \delta_{\mathsf{x}} + \mu)\,X_{\mathsf{d}}^{+}$$

Fast Ki67^{-}subset

$$\frac{dX_{\mathsf{d}}^{-}}{dt} = \beta\,X_{\mathsf{d}}^{+} - (\rho_{\mathsf{x}} + \delta_{\mathsf{x}} + \mu)\,X_{\mathsf{d}}^{+}$$

Slow Ki67^{+}subset

$$\frac{dY_{\mathsf{d}}^{+}}{dt} = \mu\,X_{\mathsf{d}}^{+} + \rho_{\mathsf{y}}\,(2\,Y_{\mathsf{d}}^{-} + Y_{\mathsf{d}}^{+}) - (\beta + \delta_{\mathsf{y}})\,Y_{\mathsf{d}}^{+}$$

Slow Ki67^{-}subset

$$\frac{dY_{\mathsf{d}}^{-}}{dt} = \mu X_{\mathsf{d}}^{+} + \beta\,Y_{\mathsf{d}}^{+} - (\rho_{\mathsf{y}} + \delta_{\mathsf{y}})\,Y_{\mathsf{d}}^{+}$$

Here, we considered that all precursor-derived cells enter the Ki67^{+} subset, since cell-division is a requisite for the commitment to the EM Treg lineage. We estimated the rates of influx (α), maturation of fast to slow subest (μ), division (ρ) and loss (δ), using the data-derived from busulfan chimeras. Additionally, we fixed the rate of loss of Ki67 expression $\beta = 1/3.5$ days^{-1}, similar to as described for the neutral and incumbent models (eq. 1 and 2).

S1C Modeling the de novo production, division and loss of naive and EM Treg

Our modeling strategy allows us to map the chimerism and Ki67 expression kinetics of the potential source population onto the dynamics of the population of interest. Specifically, the chimerism in the source constrains the parameters defining influx and 'net loss' (death - division), while the Ki67^{+} fraction of the precursor population constrains influx and division rates of the population of interest. By comparing the quality of the model fits we then established the relative support for different candidate precursors of Tregs.

Precursors of naive and EM Tregs

We considered that *de novo* generated FoxP3$^+$ thymic SP4 T cells are direct precursors of naive Tregs. For EM Tregs, we compared naive Tregs and conventional naive, central memory, and effector memory CD4 T cells as potential precursors. We describe the changes in their total pool size an donor:host chimerism using phenomenological functions described below. We use the age of the youngest animal in busulfan chimera set as the starting point for modeling *i.e.,* $t_0 = 40$ days.

Describing influx into the Treg compertments

We used a general descriptor function, described in **equation 4**, to capture the changes in the pool sizes of precursor populations of naive and EM Tregs.

$$\phi(t) = \phi_0 \, e^{-\frac{(t-t_0)}{p}}. \tag{4}$$

Our model definitions assume that rate of influx into both naive and EM Tregs 'α' remains unvarying with time and is proportional to the size of the precursor population under consideration. The rate of precursor influx is then $\alpha \times \phi(t)$, where the constant α is estimated while fitting models to the busulfan chimera data. We estimated the parameters ϕ_0 and ν by fitting **equation 4** to the log-transformed counts of the precursor population. We show the descriptions of pool size changes and parameter estimates for the precursors of naive Tregs *i.e., de novo* generated FoxP3$^+$ thymic SP4 T cells in **Fig. S1A**. We show the descriptions of pool sizes for the candidate precursors of EM Tregs *viz.* the conventional naive, central memory, and effector memory CD4 T cells in **Fig. S2A**.

Empirical descriptions of normalised chimerism in the precursor populations

We describe the changes in the fraction of donor cells in precursors of naive and EM Tregs using

$$\chi(t) = \chi_0 \left(1 - e^{-\frac{(t-t_0)^n}{q}}\right) \tag{5}$$

The parameters χ_0 and q were estimated by fitting **equation 4** to the observed time-course of donor chimerism in the precursor population in busulfan chimeras. Fits and parameter estimates for the precursor populations are shown in **Fig. S1B** and **S2B**.

Ki67 expression dynamics in the precursors of naive and EM Tregs

The fractions of Ki67 expressing cells in both the host- and donor-derived FoxP3$^+$ thymic SP4 T cells (mean values 15% and 9%, respectively) remain stable across mouse lifetime **Fig. S1C**. We assumed that these dynamics are represented in the influx into naive Tregs and fixed the rate constants ϵ_h and ϵ_d that defined Ki67$^+$ fraction in precursor influx to 0.15 and 0.09, in **equations 1** and **2.**

We assumed that all newly generated EM Tregs were Ki67$^+$, since differentiation into memory likely involves cell division.

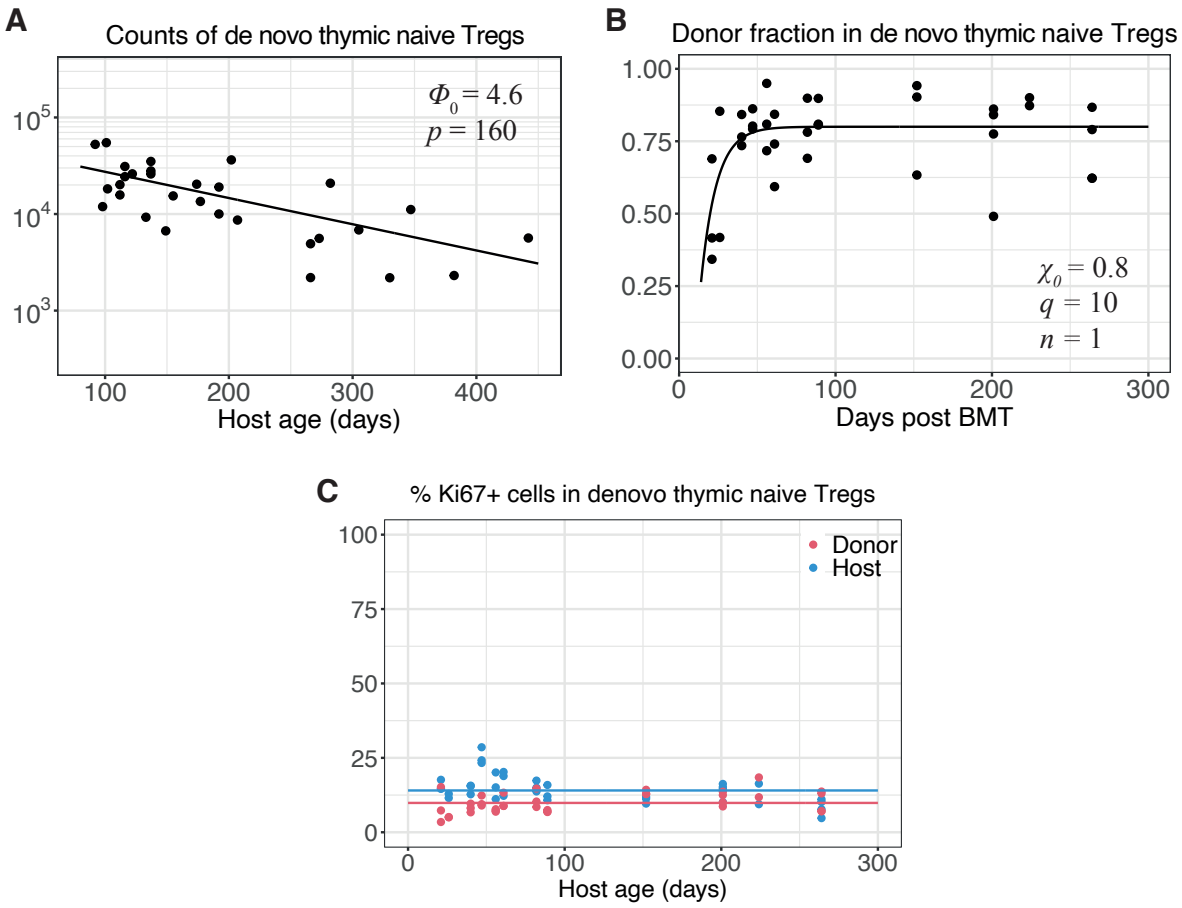

Figure S1: Dynamics of naive Treg precursors. We show the changes in pool size **(A)**, donor chimerism **(B)** and Ki67$^+$ fraction **(C)** of *de novo* generated FoxP3$^+$ thymic SP4 T cells. Curves shown in **(A)** and **(B)** were generated using **equation 4** and **equation 5**, respectively. The intercepts shown in **(C)** were fixed to the mean Ki67$^+$ percentages observed among host and donor FoxP3$^+$ thymic SP4 T cells – 15% and 9%, respectively.

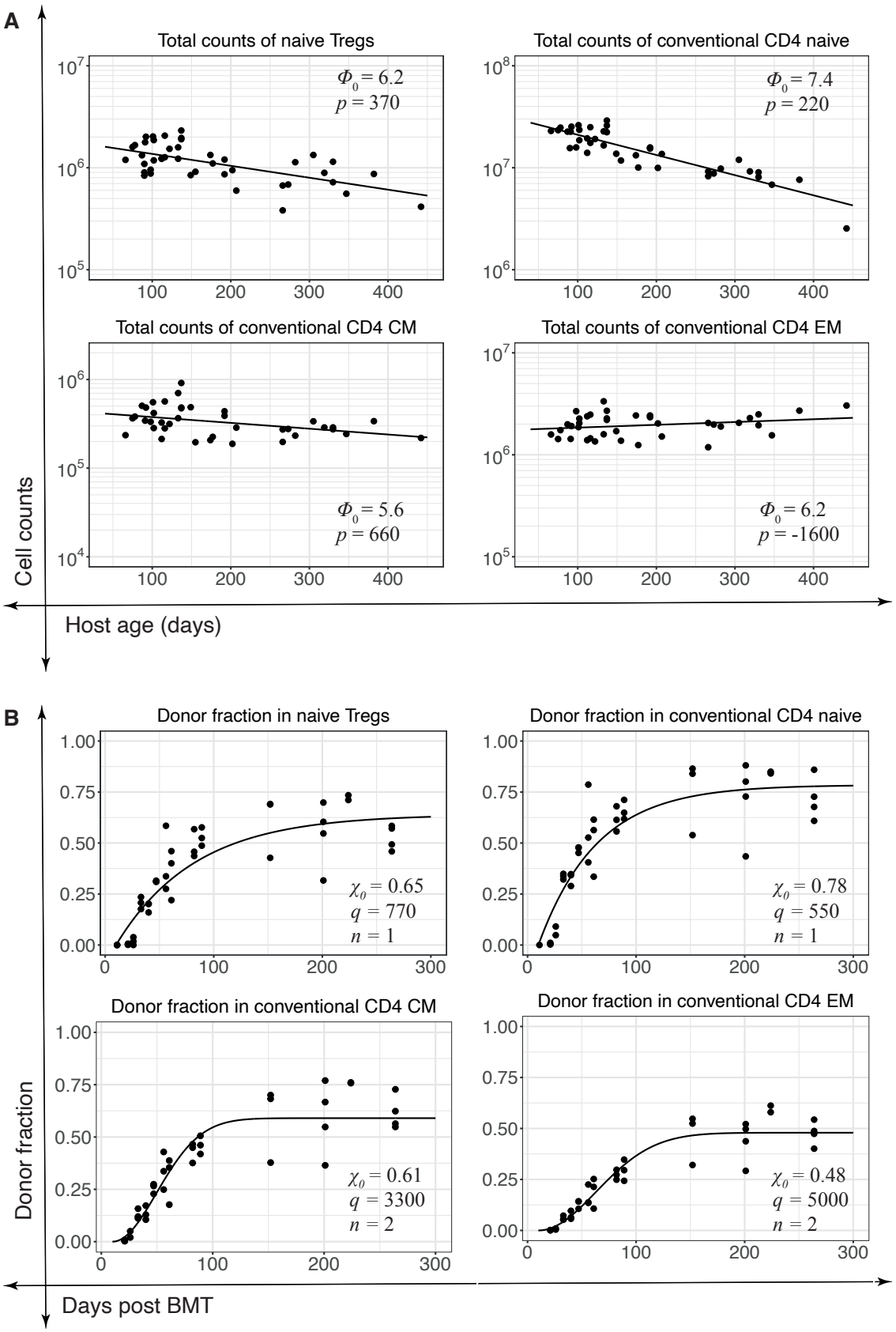

Figure S2: Dynamics of potential precursor populations of EM Tregs. We depict the time-courses of total counts **(A)** and donor chimerism **(B)** of candidate precursors of EM Treg cells. Lines shown **A** represent phenomenological descriptions of the observations of total counts (solid dots) generated using **equation 4**. Similarly, we generated curves for chimerism data in **B** using **equation 5**.

S1D Explaining the growth of EM Treg numbers over the first year of life

Our analysis suggests that EM Treg population contains a transient stage – the fast subset – which quickly transitions to a more persistent 'slow' stage with a mean time $\sim$ 5 days. The slow population divide and die on average every 40 days, but these processes are finely balanced - therefore, slow EM Treg accumulate over time as they are fed from the fast population. The growth in total EM Treg numbers during the first year of life can then be understood quite simply. If we sum Ki67$^+$ and Ki67$^-$ cells, and also sum host and donor cells, the following equations describe the timecourses of total numbers of fast (X) and slow (Y) EM Treg:

$$\frac{dX}{dt} = \alpha\,\phi(t) - (\lambda_X + \mu)X(t), \tag{6}$$

$$\frac{dY}{dt} = \mu\,X(t) - \lambda_Y Y(t), \tag{7}$$

where $\lambda_X = \delta_x - \rho_x$ and $\lambda_Y = \delta_y - \rho_y$ are the net rates of loss (that is, loss minus self-renewal) for fast and slow cells respectively. Adding these,

$$\frac{dM}{dt} = \alpha\,\phi_0 e^{-(t-t_0)/p} - \lambda_X X(t) - \lambda_Y Y(t), \tag{8}$$

where $M(t)$ is total EM Treg numbers, and we show explicitly the waning influx described empirically by the declining exponential (equation 4). Equation 8 shows that during the first year of life, when X is small, the influx of new EM cells outstrips the total rate of loss fast cells. From equation 7 we see slow cells continuously accumulate during this period, since their net loss rate λ_Y is close to zero. This accumulation explains the decline in Ki67 levels in bulk among EM Treg (Fig 4D), even while the fast cell population is increasing. Only after the influx of new EM declines sufficiently for fast cells to decline, would EM cell numbers start to fall; the model predicts this would happen in very old age, beyond the time frame of these experiments.

S2 Model validation and comparison

Each model in our modeling framework is fitted simultaneously to four sets of observations – cell counts ($y_{a,1}$), normalized donor fraction ($y_{a,2}$) and the fraction of Ki67$^+$ cells within donor ($y_{a,3}$) and host ($y_{a,4}$) cells, where a denotes the animal (a = 1,…,n).

We estimate the model parameters using a Bayesian statistical inference approach. The joint density of the observations in each animal is defined as, $y_a = (y_{a,1}, y_{a,2}, y_{a,3}, y_{a,4})$. We assume that y_a have independent multivariate normal distributions with mean $\mu_a = (\mu_{a,1}, \mu_{a,2}, \mu_{a,3}, \mu_{a,4})$ and covariance matrix $D = \text{diag}(\sigma_1^2, \sigma_2^2, \sigma_3^2, \sigma_4^2)$. Here, $\mu_{a,i} = f_i(time_a, \theta)$, is the model prediction for i^{th} observation in a^{th} animal. The 'prior' distributions of model parameters are defined based on existing knowledge regarding their values. Observations from the posterior distribution of (θ, D) are generated using the no-U-turn-sampler sampler in the *Stan* language, where parameters are sampled from the joint prior density following the Hamiltonian Monte Carlo algorithm.

Model selection criteria: We estimate the expected log point-wise predictive density (elpd^j) for each model (M_j), which is the measure of its performance and out-of-sample prediction accuracy [1,2], using the leave-one-out (LOO) cross validation method. The LOO process estimates the probability density $P(y_i|y_{-i}, M_j)$ of the prediction of i^{th} observation using the model M_j fitted on the data with observation i excluded. The elpd estimate is then the sum of the predictive densities of the LOO estimates of all n observations in the data,

$$\widehat{\text{elpd}^j_{\text{loo}}} = \sum_{i=1}^{n} \text{elpd}^j_{\text{loo, i}} = \sum_{i=1}^{n} \log(P(y_i|y_{-i}, M_j), \qquad \text{se}(\widehat{\text{elpd}^j_{\text{loo}}}) = \sqrt{\sum_{i=1}^{n} \left(\text{elpd}^j_{\text{loo, i}} - \text{elpd}^j_{\text{loo}}/n\right)^2}. \tag{9}$$

We use the estimates of elpd and its standard error (eq. 9) to calculate the relative support for each model as the model weight (W) and to rank them using the Pseudo-Bayesian model averaging method, implemented in the *loo* package in *R*.

$$W_j = \frac{\exp\left(\widehat{\text{elpd}^j_{\text{loo}}} - \frac{1}{2}\text{se}(\widehat{\text{elpd}^j_{\text{loo}}})\right)}{\sum_{j=1}^{J} \exp\left(\widehat{\text{elpd}^j_{\text{loo}}} - \frac{1}{2}\text{se}(\widehat{\text{elpd}^j_{\text{loo}}})\right)}. \tag{10}$$

As the elpd estimates are derived from LOO cross validation, W is interpreted as the confidence in a model's ability to predict new data, relative to all the other models under consideration.

References

1. Vehtari, A., Gelman, A. and Gabry, J. (2016). Practical Bayesian model evaluation using leave-one-out cross-validation and WAIC. Statistics and Computing *27*, 1413–1432.

2. Yao, Y., Vehtari, A., Simpson, D. and Gelman, A. (2018). Using Stacking to Average Bayesian Predictive Distributions (with Discussion). Bayesian Analysis *13*.

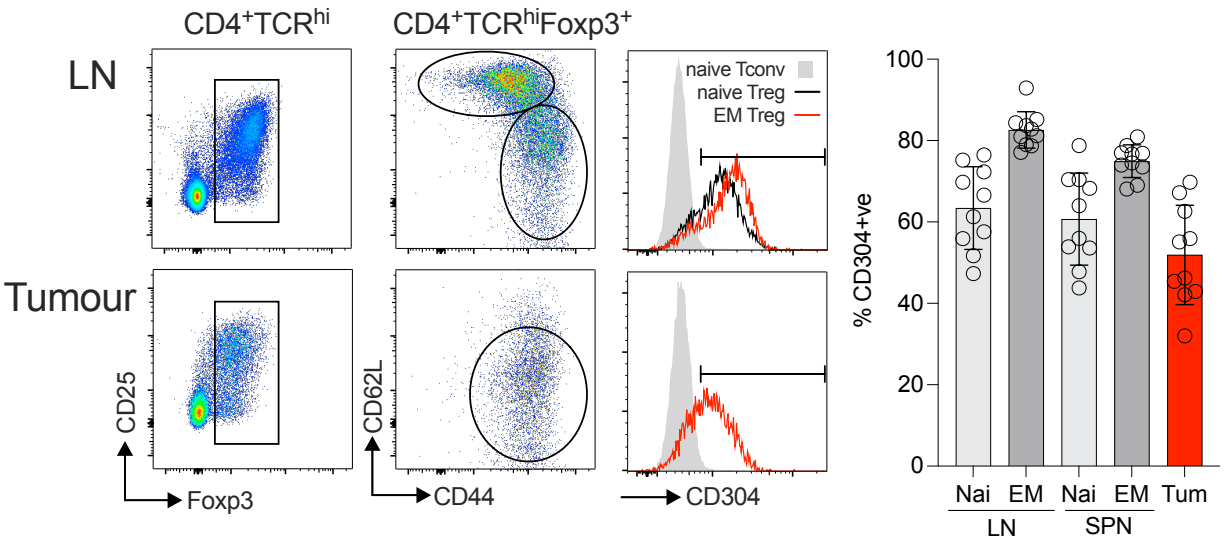

Figure S3 - **Nrp1 (CD304) expression by circulating and intratumoral Treg.** Treg from lymph nodes and tumours of busulfan chimeras described in figure 7C, engrafted with MC38 cells, were analysed for expression of CD304. Density plots show gating strategy to identify Foxp3+ Treg, and naive vs EM Treg subsets therein. Histograms show CD304 expression by naive and EM Treg from LN (as compared with naive CD4+ conventional T cells (TOP histogram), and EM Treg in tumour vs naive CD4+ conventional T cells from LN. Summary bar charts show % CD304+ in the indicated Treg subsets in LN, spleen and tumour (n=9 pooled from three experiments).